Understanding Urea Oxidation Reaction Kinetics in Nickel Based Electrocatalysts

Phillip Victor Torres Romero

A thesis

submitted in partial fulfillment of the

requirements for the degree of

Master of Science

University of Washington

2025

Committee:

Eric Stuve

Stuart Adler

Program Authorized to Offer Degree:

Chemical Engineering

University of Washington

Abstract

Understanding Urea Oxidation Reaction Kinetics in Nickel Based Electrocatalysts

Phillip Victor Torres Romero

Chair of the Supervisory Committee:

Eric Stuve

Department of Chemical Engineering

This study investigates the electrochemical oxidation of urea on nickel electrodes in alkaline media. Using cyclic voltammetry (CV), the influence of urea concentration and applied potential on the redox transitions of $Ni(OH)_2$/NiOOH was explored. The results reveal that β-NiOOH is critical as a catalytic oxidant in the indirect oxidation mechanism, with increasing urea concentrations leading to suppression of the β-NiOOH reduction peak. Cathodic area analysis visualizes the extent of the suppression in the presence of urea. Fixed-potential analyses indicate kinetic inhibition at elevated concentrations due to surface saturation or adsorption effects. Kinetic modeling based on surface coverage supports a potential-dependent transition from electrochemical to chemically limited regimes. These findings provide a foundation for future optimization of nickel-based electrocatalysts for energy-efficient hydrogen production and urea-rich wastewater treatment.

Chapter 1

Introduction

In the year 2024, the world recorded the warmest year on record since started in 1850. Earth's temperature has risen an average of 0.11° Fahrenheit every decade since 1850 and has now reached over 2.63° Fahrenheit above the pre-industrialization average. [1] The largest contributing factor to this rise of temperature is the release of carbon and other major greenhouse gases due to human activity. This has led to a large increase in scientific research on the reduction of greenhouse emissions from large energy sources. Governments, research institutions, and private companies worldwide have significantly ramped up investment in decarbonization technologies and strategies.[1] Alternative energy sources such as renewable wind and solar have seen great innovations as well as the field of energy storage with batteries. One potential energy storage solution is using hydrogen.

As an energy carrier rather than a primary source, hydrogen offers unique advantages for storing renewable energy over extended periods, addressing the intermittency challenge of wind and solar generation. "Green hydrogen," produced through electrolysis powered by renewable electricity, creates no direct emissions and can be stored for months without degradation. This versatile element can be used directly in fuel cells to generate electricity, blended into natural gas pipelines, or employed in industrial processes that currently rely on fossil fuels. Hydrogen's high energy density makes it particularly valuable for decarbonizing sectors resistant to direct electrification, such as steel production, long-haul shipping, and aviation as visualized in Figure 1.1. Despite challenges in production efficiency, transportation infrastructure, and cost, significant investment in hydrogen technologies suggests it may play a crucial role in achieving net-zero emissions targets by mid-century. Hydrogen production has historically relied on methods like steam methane reforming and coal gasification, which generate significant carbon emissions. Water electrolysis offers a cleaner alternative but requires substantial energy input. Recently, urea has emerged as a promising hydrogen source through electrochemical oxidation.

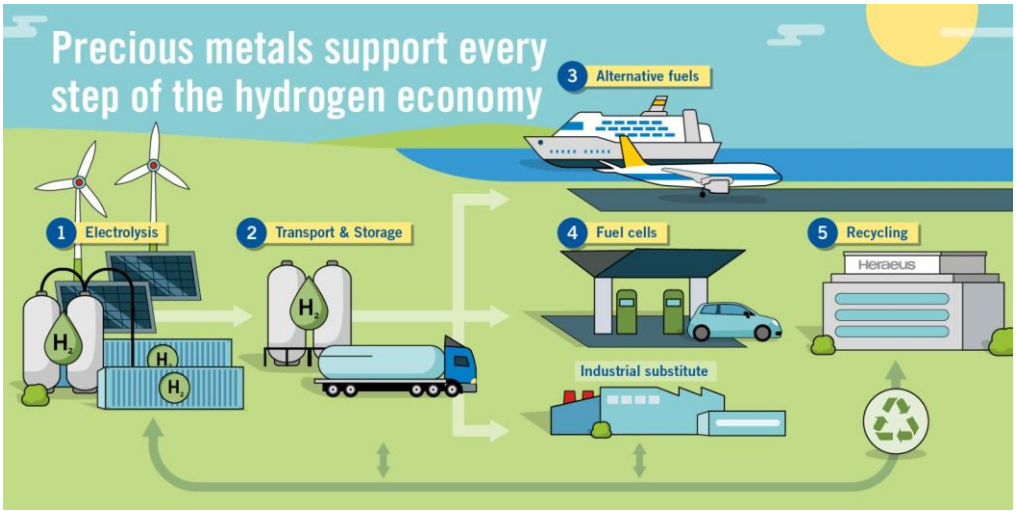

Figure 1.1 Hydrogen Economy Overview[2]

Urea is a clear, odorless organic compound that is a major byproduct of mammalian protein metabolism, formed primarily in the liver through the urea cycle. Its widespread utility stems from its rich nitrogen content, making it an indispensable component in agricultural fertilizers. Beyond agriculture, urea also finds diverse applications in medicine (as a diuretic and dermatological treatment), textiles (as a component in dyeing processes), cosmetics (as a skin moisturizer), and chemical manufacturing. Despite its broad utility, the improper disposal of urea-rich wastewater has emerged as a serious environmental concern. When discharged into the environment, urea decomposes into ammonia, a toxic compound that can volatilize into the atmosphere or leach into groundwater systems. The presence of excess ammonia in water bodies contributes to eutrophication, leads to oxygen depletion, and poses direct threats to human and aquatic health as shown in Figure 1.2. Consequently, the search for effective methods to mitigate urea pollution has intensified. Electrocatalysis, a technique that utilizes electrochemical reactions facilitated by catalysts, has recently attracted considerable attention as a promising approach to decompose urea in wastewater. This process not only purifies contaminated water by breaking urea down into benign products such as nitrogen gas and carbon dioxide but also enables the generation of hydrogen gas. [3,4]

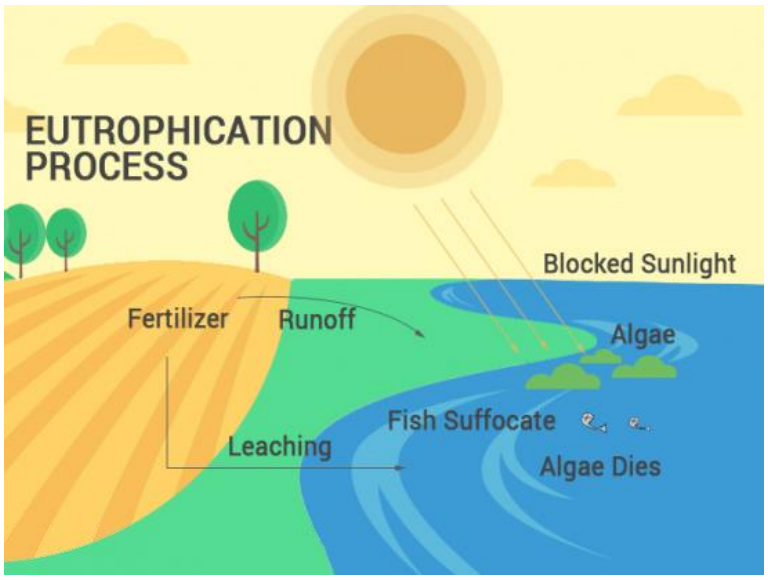

Figure 1.2 Eutrophication Process, nitrogen entering water stream[5]

In the broader quest for sustainable and decentralized energy production, the utilization of wastewater as a resource, particularly urea-rich wastewater, has gained substantial interest. Urea typically constitutes about 2–2.5 wt.% of human and animal urine and is prevalent in municipal wastewater streams, making it an abundant and underutilized source of chemical energy. Additionally, urea is produced on an industrial scale for fertilizers, with global production exceeding 180 million tons annually, further contributing to its widespread presence in waste effluents.[3] The natural microbial degradation of urea in the environment leads to the formation of nitrates and nitrites, which are associated with several health risks. Traditional denitrification methods, which aim to remove these hazardous compounds from wastewater, are often energy-intensive, costly, and inefficient, relying on large chemical inputs or complex biological treatment systems. These limitations underscore the urgent need for innovative, cost-effective technologies that can simultaneously address both environmental and energy challenges.

Urea electrolysis has emerged as a highly promising method for achieving both wastewater purification and renewable hydrogen production in a single integrated process. In this technique, urea molecules undergo electrochemical oxidation at the anode of an electrolytic cell, leading to the formation of environmentally benign products such as nitrogen gas and carbon dioxide. Simultaneously, at the cathode, water reduction reactions produce high-purity hydrogen

gas, which can be captured and stored as a clean energy resource. The net reaction for urea oxidation is thermodynamically more favorable than water splitting alone, requiring a lower operating potential (~0.37 V vs. ~1.23 V for water electrolysis), thereby offering substantial energy savings. Furthermore, the electrolysis process generates clean water as a by-product, contributing to water resource recovery. Integrating urea electrolysis into existing wastewater treatment facilities could revolutionize how communities manage waste and produce renewable fuels, providing a cost-effective alternative to traditional denitrification processes. This synergy between environmental remediation and energy generation represents a critical advancement toward the development of circular, sustainable technologies aimed at mitigating both pollution and energy scarcity challenges.

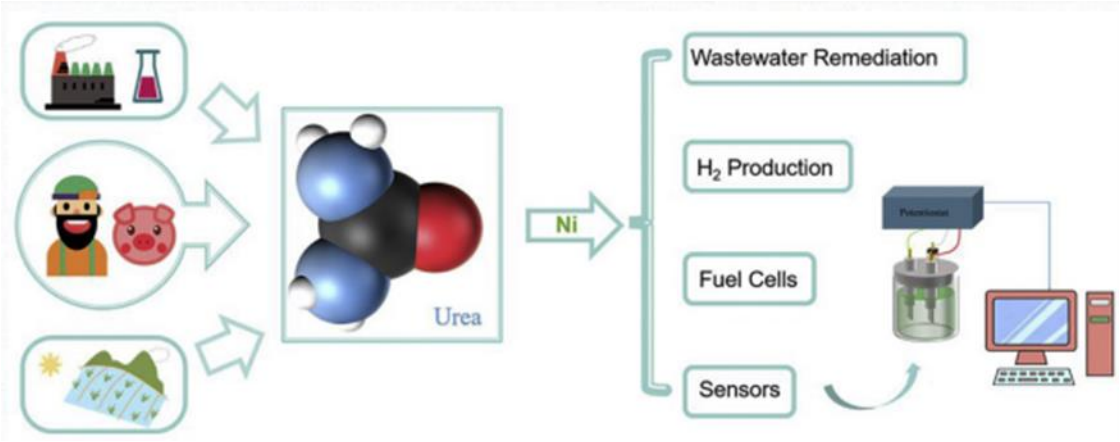

Figure 1.3 Applications of the Electrooxidation of Urea [3]

The practical applications extend beyond municipal wastewater treatment to include agricultural settings where animal waste management presents significant challenges. Concentrated animal feeding operations generate enormous volumes of urine-rich waste that could serve as feedstock for hydrogen production while mitigating pollution risks. Similarly, industrial facilities that produce urea-containing effluents, such as fertilizer manufacturing plants, could benefit from on-site urea electrolysis systems that convert waste streams into valuable hydrogen.

Looking forward, several challenges must be addressed to realize the full potential of urea electrolysis. These include scaling up laboratory demonstrations to commercial-scale

operations, improving catalyst longevity and performance under real-world conditions, developing cost-effective cell designs, and optimizing system integration with existing infrastructure. Additionally, the economics of urea-to-hydrogen conversion will depend on policy frameworks, carbon pricing mechanisms, and the valuation of multiple benefits beyond energy production, including pollution reduction and water treatment.

Research efforts are increasingly focusing on developing integrated systems that can handle complex real-world wastewater applications rather than idealized solutions. Innovative approaches combining biological pre-treatment with electrochemical processes show promise for handling variable waste compositions and concentrations. Meanwhile, advances in materials science continue to yield improved catalysts and electrode materials that enhance system efficiency and durability while reducing costs.

The transformation of urea from an environmental liability to a valuable resource for hydrogen production represents a compelling example of circular economy principles applied to waste management and energy production. As technology advances and environmental regulations become more stringent, urea electrolysis stands poised to make significant contributions to sustainable development goals, addressing simultaneously the challenges of waste management, water pollution, and clean energy production.

The process of urea electrolysis involves a six-electron transfer processes with sluggish kinetics at the anode, which significantly impacts the efficiency of the process. This multi-electron oxidation reaction creates substantial activation barriers, resulting in high overpotentials when using conventional electrode materials. The six-electron transfer mechanism proceeds through several intermediate steps, potentially involving adsorbed species like $-NH_2$, -NH, and -NO, before completing the oxidation to nitrogen. The rate-determining step often involves the breaking of C-N bonds or the formation of nitrogen-nitrogen bonds, both energetically demanding processes that contribute to the overall sluggish reaction kinetics.

Improving the kinetics of urea electrooxidation is crucial for enhancing urea electrolysis efficiency and commercial viability. Effective catalysts must facilitate multiple aspects of the reaction: they must adsorb urea molecules at appropriate binding strengths, activate the relevant bonds, stabilize reaction intermediates, and efficiently transfer electrons. The catalyst surface

structure plays a critical role, with specific crystal facets and surface defects offering preferential reaction sites. Furthermore, the catalyst must maintain active in strongly alkaline conditions (typically pH > 13) where urea electrolysis occurs most efficiently.

Although precious metals and their oxides like platinum, rhodium, and iridium dioxide exhibit high conductivity and excellent electrocatalytic activity, especially in alkaline media, their practical application is hindered by scarcity, high cost, and low mechanical strength. These noble metal catalysts, while offering superior electron transfer properties and resistance to corrosion, represent an economic bottleneck for large-scale implementation. A kilogram of platinum currently costs around $30,000, making electrode materials prohibitively expensive for wastewater treatment applications. Additionally, these materials often suffer from poisoning by reaction intermediates or contaminants present in real wastewater, further limiting their practical utility.

Catalyst Material	Approximate Price (USD/kg)	Relative Cost Factor (compared to Nickel)	Key Applications in Electrocatalysis
Platinum (Pt)	$30,000 - $35,000	~1,500×	High-performance electrodes, fuel cells, fine chemical synthesis
Rhodium (Rh)	$150,000 - $200,000	~8,750×	Specialized electrodes, automotive catalysts, nitrogen oxide reduction
Iridium Dioxide (IrO_2)	$80,000 - $100,000	~4,500×	Dimensionally stable anodes, oxygen evolution reaction, chlor-alkali production
Nickel (Ni)	$20 - $25	1×	Urea electrolysis, hydrogen evolution, alkaline electrolyzers

Table 1. Cost of Electrocatalytic Metals for Urea Oxidation

Consequently, the search for low-cost, high-activity non-precious metal catalysts has become a research priority in the field. This pursuit reflects broader efforts in electrochemistry to develop earth-abundant alternatives to precious metal catalysts. The ideal catalyst would combine high electrocatalytic activity with durability, resistance to poisoning, and cost-

effectiveness, a challenging combination of properties that continues to drive innovation in materials science.

Nickel has been extensively studied and used in modified electrodes for its electrocatalytic properties in the oxidation of various organics, including methanol, ethanol, glucose, cyclohexanol, and aspirin.[3] Its particular effectiveness for urea oxidation stems from the catalytic properties of its oxidized forms, especially nickel oxyhydroxide (NiOOH), which forms in situ on nickel surfaces during anodic polarization in alkaline media. The Ni^{2+}/Ni^{3+} redox couple plays a crucial role in the electrocatalytic mechanism, with Ni^{3+} species functioning as electron transfer mediators that facilitate urea oxidation.

Despite these advances, challenges remain in developing nickel-based catalysts that maintain high activity over extended periods in the harsh conditions of real wastewater treatment applications. Catalyst deactivation through mechanisms such as surface poisoning, dissolution, and structural changes remains a significant hurdle for practical implementation.

Chapter 2

Literature Review

2.1 Urea Overview

Urine is the most abundant form of human and animal waste on Earth and represents a major component of municipal wastewater streams.[6,7] One of the primary constituents of urine is urea, a simple organic compound with the molecular formula $CO(NH_2)_2$. In fresh human urine, urea typically makes up about 2–2.5 wt.% or roughly 0.33 M in concentration.[6] This high prevalence stems from urea's biological role as the main nitrogenous waste product of protein metabolism in mammals, synthesized in the liver via the urea cycle and excreted by the kidneys.[6]

Chemically, as shown in Figure 2.1, urea is composed of carbon, nitrogen, hydrogen, and oxygen, four key elements that make it not only a significant pollutant when released unchecked into the environment but also a potentially valuable feedstock for energy applications.[3,6,7] Urea is a hydrogen-rich compound, containing approximately 6.7 wt% hydrogen, and possesses a relatively high energy density of 16.9 MJ L^{-1}, making it an attractive candidate for energy applications. It is chemically stable under ambient environmental conditions, non-toxic, and non-flammable, which facilitates safe storage and transportation.[3] As urea-containing wastewater enters natural water bodies, microbial activity leads to its decomposition, producing ammonia and contributing to environmental nitrification, which can cause harmful algal blooms, oxygen depletion, and aquatic ecosystem disruption.

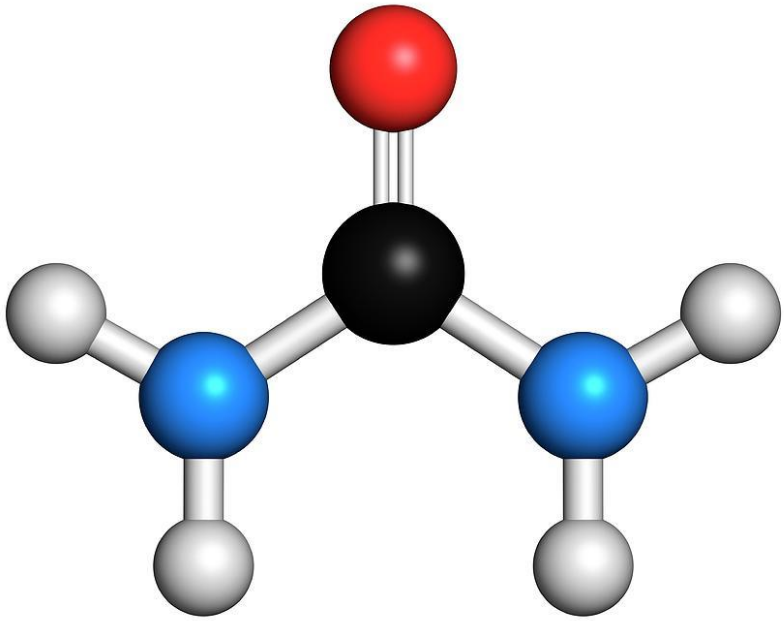

Figure 2.1 Urea Molecule, composed of carbon (black), oxygen (red), nitrogen (blue), and hydrogen (grey)[8]

However, this same compound, once considered merely waste, has garnered increasing interest for its potential in sustainable energy systems. Because each molecule of urea contains four hydrogen atoms and two nitrogen atoms, it presents a renewable and accessible source of hydrogen gas when decomposed electrochemically. Recent research has focused on developing technologies to recover urea from municipal wastewater not only to mitigate its environmental impacts but also to repurpose it as a precursor for clean hydrogen production through urea electrolysis.[6,7] This dual benefit, waste remediation and energy generation, makes urea a focal point in the nexus of environmental management and green energy innovation.

2.2 Urea Electrolysis

The Urea Oxidation Reaction (UOR) has been seen as the most efficient way to produce hydrogen in either wastewater or urine.[7] In urea electrolysis, urea is electrochemically oxidized at the anode, where it undergoes a six-electron transfer process that ultimately yields nitrogen gas (N_2) and carbon dioxide (CO_2) as the primary gaseous products at the anode and hydrogen

gas (H_2) evolved as the primary gaseous product at the cathode. The following shows the electrooxidation of urea in alkaline medium using a nickel catalyst at the anode.

Anode:

$$CO(NH_2)_{2(aq)} + 6OH^- \rightarrow N_{2(g)} + 5H_2O_{(l)} + CO_{2(g)} + 6e^- \quad (2.1)$$

$$Ni(OH)_{2(s)} + OH^- \rightleftharpoons NiOOH_{(s)} + H_2O_{(l)} + e^- \quad (2.2)$$

Cathode:

$$6H_2O_{(l)} + 6e^- \rightarrow 3H_{2(g)} + 6OH^- \quad (2.3)$$

Overall:

$$CO(NH_2)_{2(aq)} + H_2O_{(l)} \rightarrow N_{2(g)} + 3H_{2(g)} + CO_{2(g)} \quad (2.4)$$

Urea undergoes electrochemical oxidation at the anode as shown in equation 2.1 with a standard electrode potential of 0.46 V vs. SHE. The Gibbs free energy of urea is determined by summing the crystalline Gibbs energy and the energy required for its dissolution into solution. First, the crystalline Gibbs free energy of urea corresponds to its standard-state free energy in the solid phase. This value reflects the intrinsic thermodynamic stability of urea in its most ordered, low-entropy form and encompasses the enthalpic and entropic factors associated with the formation and maintenance of the crystalline lattice structure. It serves as the thermodynamic reference point for solid-phase urea under standard conditions. Second, the Gibbs free energy of dissolution quantifies the energetic cost associated with transferring urea from the solid phase into the aqueous phase. This step involves the disruption of the crystal lattice, which requires energy to overcome the intermolecular forces holding the solid together. Simultaneously, it accounts for the hydration and solvation of urea molecules as they interact with surrounding water molecules in solution. The net change in free energy for this process depends on the temperature, ionic strength, and the specific interactions between urea and the solvent. It is this dissolution component that determines the chemical potential of urea in its reactive form within an aqueous electrolyte.

Concurrently, the oxidation of nickel hydroxide ($Ni(OH)_2$) to nickel oxyhydroxide (NiOOH) is shown in equation 2.2. This reaction occurs at a slightly higher potential of 0.49 V

vs. SHE. On the cathode, water undergoes alkaline reduction as shown in equation 2.3, producing hydrogen gas at a standard potential of 0.83 V vs. SHE. Collectively, the full-cell reaction for urea electrolysis of equation 2.4 requires a thermodynamic cell voltage of only 0.37 V under standard conditions. This is markedly lower than the 1.23 V required for conventional water electrolysis, suggesting that hydrogen production via urea electrolysis could be up to 70% more energy-efficient and cost-effective, highlighting its potential for energy-efficient hydrogen production.[6] Lastly, the nitrogen produced at the anode shows the denitrification potential of urea electrooxidation thereby remediating wastewater whilst producing hydrogen.[6]

2.3 Nickel-Based Catalysts in Alkaline Medium

Nickel, owing to its high natural abundance, relatively low cost, and favorable electronic structure, has emerged as one of the most versatile transition metals in catalysis. It is well established that nickel can act as an effective catalyst due to its surface oxidation properties, particularly its ability to undergo redox transitions between Ni, Ni^{2+}, and Ni^{3+} states.[9–11] These redox transformations facilitate the formation of catalytically active species capable of promoting a wide range of electrochemical reactions, especially in alkaline environments.

One particularly important application of nickel in electrocatalysis is in the oxidation of small organic molecules, including alcohols and urea.[10] Electrooxidation studies on nickel have demonstrated its catalytic efficiency in alcohol oxidation, including methanol and ethanol, where the formation of higher valence nickel oxides (such as NiOOH) plays a pivotal role.[10] For instance, Van Effen and Evans (25) highlighted that ethanol oxidation in alkaline media proceeds through the formation of these higher valence states, which act as chemical oxidants for the alcohol substrates.[10,12] Cyclic voltammetry and impedance spectroscopy have provided further mechanistic insights, confirming that NiOOH participates in a mediated electron transfer process with organic reactants.

Beyond alcohol oxidation, the versatility of nickel as a non-noble catalyst has gained considerable attention for methanol oxidation reaction (MOR), particularly in direct methanol fuel cells (DMFCs).[11] Among the transition metals, nickel exhibits high catalytic activity and commendable resistance to poisoning intermediates such as CO, making it a promising alternative to platinum-group metals. The facile interconversion of Ni, Ni^{2+}, and Ni^{3+} species promotes the formation of reactive intermediates such as NiOOH, accelerating the MOR in

alkaline conditions.[11] Since the pioneering work in the 1950s involving porous nickel electrodes, extensive research has led to the development of a broad spectrum of nickel-based materials for MOR. These include layered double hydroxides (e.g., $Ni(OH)_2$), nickel coordination complexes, bimetallic alloys (such as NiCu and NiCo), and carbon-supported nickel nanoparticles.[11]

The evolution of nickel-based electrocatalysts over the past decade has seen significant improvements in both structural design and catalytic efficiency. Advanced morphologies, such as core-shell architectures, heterostructures, and composite hybrids, have enabled enhanced surface area, synergistic interfacial effects, and improved electron transport, all of which contribute to superior catalytic performance.[11]

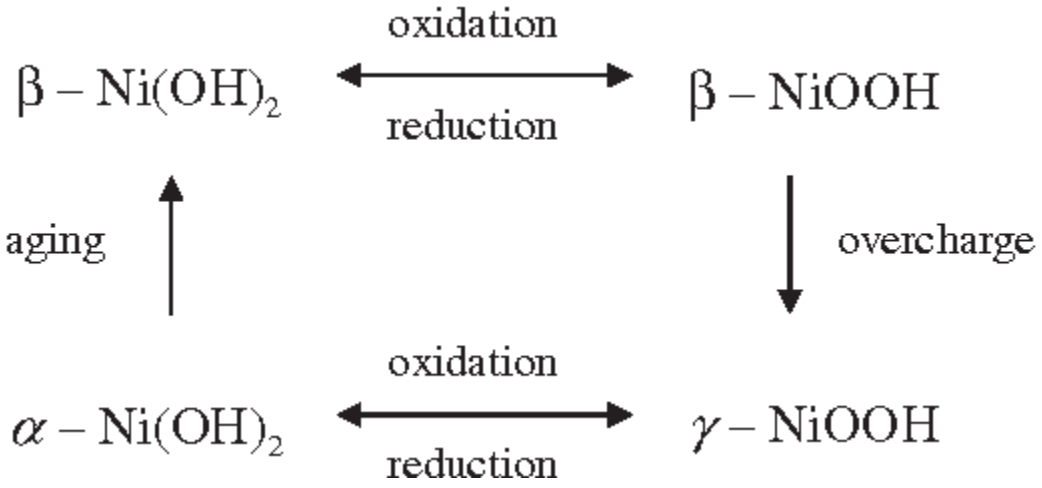

Figure 2.2 Phase Transformations of Nickel Hydroxides [13]

The main electrochemical process occurring at low potentials on nickel surfaces involves the reversible oxidation of Ni to form surface α-$Ni(OH)_2$ during the anodic sweep, followed by its reduction during the cathodic sweep.[9] This α-$Ni(OH)_2$ is believed to grow via the formation of three-dimensional islands, with intercalated water molecules, as evidenced by in situ scanning tunneling microscopy and low-temperature cyclic voltammetry. According to the place-exchange model, its formation involves three steps: (1) adsorption of OH^- onto the Ni surface forming Ni–OH_{ad} (eqn 2.5), (2) incorporation of OH into the subsurface to create a quasi-3D lattice between Ni layers (eqn 2.6), and (3) chemisorption of a second monolayer of OH on this intermediate structure (eqn 2.7).[9]

α-$Ni(OH)_2$ Formation:

$$Ni + OH^- \rightleftarrows Ni - OH_{ad} + e^- \quad (2.5)$$

$$Ni - OH_{ad} \rightleftarrows (OH - Ni)_{quasi-3D\ lattice} \quad (2.6)$$

$$(OH - Ni)_{quasi-3D\ lattice} + OH^- \rightleftarrows Ni(OH)_{2,ad} + e^- \quad (2.7)$$

In the high-potential region (0.5–1.2 V vs RHE), α-$Ni(OH)_2$ undergoes irreversible dehydration and transforms into β-$Ni(OH)_2$, often accompanied by the formation or thickening of NiO.[9] This transformation suppresses the cathodic peak at low potentials, eventually leading to its complete disappearance once β-$Ni(OH)_2$ fully covers the electrode. As the potential exceeds 1.2 V vs RHE, α-/β-$Ni(OH)_2$ further oxidizes to γ-/β-NiOOH, evidenced by a new anodic peak around 1.4 V and a cathodic peak near 1.3 V, often split due to the coexistence of β- and γ-NiOOH phases.[9] At potentials above 1.5 V, the electrode surface becomes dominated by NiOOH and NiO layers, confirmed by in situ Raman and XPS studies. No clear crystal orientation effects are observed at these high potentials, likely due to rapid surface disordering.[9]

Studies have also been done by seeing the effect of temperature and scan rate on the nickel transition. For example, Alsabet et al produced cyclic voltammetry (CV) profiles of a Ni(poly) electrode across a temperature window of 281–313 K.[14] They observed anodic peak shifts toward lower potentials with increasing temperature, while the cathodic peak potential remains largely unaffected. Notably, a pronounced increase in the anodic peak current density (j_{peak}) is evident with temperature elevation, whereas the cathodic peak shows only a minor enhancement. Furthermore, the CV profiles indicated a temperature-dependent increase in current associated with the oxygen evolution reaction (OER), suggesting that the enhanced anodic current at elevated temperatures likely arises from the simultaneous contributions of β-NiOOH formation and OER.[14]

Alsabet et al. also found that increasing the scan rate led to a higher current density (j), accompanied by a progressive shift of the anodic peak toward more positive potentials and the cathodic peak toward more negative potentials.[14] Consequently, peak separation widened with increasing scan rate. Additionally, the anodic peak consistently exhibited a slightly higher charge density than the cathodic peak, indicating that more β-NiOOH was formed than reduced during the CV cycle. At low scan rates, the anodic transient featured a single peak, while the cathodic transient showed one peak accompanied by a shoulder, suggesting the presence of a secondary,

overlapping reduction event. Supporting data from electrochemical quartz crystal microbalance (EQCM) studies using electrodeposited Ni revealed an increase in interfacial mass upon reduction of anodically generated β-NiOOH back to β-$Ni(OH)_2$.[14] At higher scan rates, both anodic and cathodic transients displayed a single, well-defined peak, and in both low and high scan rate regimes, no significant features were observed within the 0.50–1.20 V range, where current densities remained minimal. Repeated potential cycling within the 0.50–1.60 V window at constant scan rate resulted in a progressive increase in the charge densities of both anodic and cathodic peaks.[14]

2.4 Urea Reaction Mechanisms with Nickel-Based Catalysts

In alkaline media, the UOR proceeds through two primary mechanistic pathways: (I) direct oxidation, and (II) indirect oxidation via catalyst regeneration.[3,6] The direct pathway involves the immediate electrochemical oxidation of urea at the electrode surface, whereas the indirect pathway includes the oxidation and subsequent regeneration of the electrocatalyst, typically a transition metal hydroxide. Both mechanisms rely on NiOOH on the surface of the electrode.

The direct mechanism of UOR in alkaline media involves the catalytic activity of nickel-based materials, particularly $Ni(OH)_2$/NiOOH redox couples. In this pathway, $Ni(OH)_2$ is electrochemically oxidized in a single step to NiOOH, which serves as the active catalytic species. Unlike the indirect mechanism, where NiOOH undergoes a chemical reduction by urea, the direct mechanism entails the simultaneous oxidation of urea and the electrochemical formation of NiOOH, with no intermediate regeneration step. Once formed, NiOOH directly catalyzes the oxidation of urea, leading to its decomposition into nitrogen (N_2), carbon dioxide (CO_2), and water (H_2O).[3,7]

Direct Mechanism on Anode:

$$6Ni(OH)_{2(s)} + 6OH^- \rightleftharpoons 6NiOOH_{(s)} + 6H_2O_{(l)} + 6e^- \quad (2.8)$$

$$CO(NH_2)_{2(aq)} + 6OH^- \rightarrow N_{2(g)} + 5H_2O_{(l)} + CO_{2(g)} + 6e^- \quad (2.9)$$

The indirect oxidation mechanism of UOR involves a redox cycle between nickel hydroxide and nickel oxyhydroxide. In this pathway, $Ni(OH)_2$ is first electrochemically oxidized

to NiOOH, which subsequently reacts with urea, reducing back to $Ni(OH)_2$ while simultaneously oxidizing urea to nitrogen (N_2) and carbon dioxide (CO_2).[3,7] Experimental studies have shown that a critical concentration of Ni^{3+} species on the electrode surface is necessary to initiate significant urea oxidation.[3] The reaction mechanism exhibits a dependence on urea concentration: at low concentrations, the process is primarily diffusion-controlled, whereas at higher concentrations, kinetic factors dominate. These findings support an EC' mechanism, wherein NiOOH is chemically reduced by urea and electrochemically regenerated, establishing a catalytic redox cycle essential for sustained urea oxidation.[3,7]

Indirect Mechanism on Anode:

$$6Ni(OH)_{2(s)} + 6OH^- \rightleftharpoons 6NiOOH_{(s)} + 6H_2O_{(l)} + 6e^- \quad (2.10)$$

$$6NiOOH_{(s)} + CO(NH_2)_{2(aq)} + H_2O_{(l)} \rightarrow 6Ni(OH)_{2(s)} + N_{2(g)} + CO_{2(g)} \quad (2.11)$$

Net Anodic Reaction:

$$CO(NH_2)_{2(aq)} + 6OH^- \rightarrow N_{2(g)} + 5H_2O_{(l)} + CO_{2(g)} + 6e^- \quad (2.12)$$

The oxygen evolution reaction (OER) is a competing anodic process that occurs at more positive potentials during electrochemical experiments conducted in alkaline media. The evolution of one oxygen molecule via OER necessitates the transfer of four electrons, making it inherently more complex than many other electrochemical processes. As a result, OER is characterized by sluggish kinetics and requires a substantial energy input to overcome the high activation barrier associated with the multistep electron transfer and bond-breaking processes.[15] The onset of OER typically begins around 1.6 V vs. RHE or 0.65 V vs. Hg/HgO. Most studies set a limitation to potential sweeps in order to maximize the selectivity and efficiency of the urea oxidation reaction (UOR) by preventing OER from consuming current and occupying active catalytic sites on the electrode surface.[7]

Oxygen Evolution Reaction:

$$4OH^- \rightarrow O_{2(g)} + 2H_2O_{(l)} + 4e^- \quad (2.13)$$

OER competes with UOR for the same Ni-based catalytic sites, particularly the high-valent Ni^{3+} species (e.g., NiOOH) that are also critical for urea oxidation. When the potential

exceeds the OER threshold, hydroxide ions (OH^-) are oxidized to oxygen gas (O_2), which reduces the effective catalytic surface area available for urea molecules and thereby diminishes UOR efficiency. Interestingly, experimental observations reveal that in the presence of urea, the onset of OER shifts toward more positive potentials.[7] This potential shift is likely attributed to the preferential adsorption of urea molecules over OH^- on the Ni^{3+} active sites, effectively delaying the OER and allowing UOR to dominate over a broader potential window. This phenomenon highlights the competitive adsorption dynamics between urea and hydroxide ions on the electrode surface and underscores the importance of potential control in optimizing UOR while suppressing parasitic reactions such as OER.

2.5 Incidental Iron

In a study by Trotochaud et al., the group explored the complex role of iron (Fe) in the performance of nickel-based (Ni-based) electrocatalysts for the oxygen evolution reaction (OER). The researchers conducted a comprehensive investigation using electrochemical methods, in situ electrical conductivity measurements, photoelectron spectroscopy, and X-ray diffraction on thin films of $Ni_{1-x}Fe_x(OH)_2$/$Ni_{1-x}Fe_xOOH$. A novel method was developed to rigorously purify KOH electrolyte by removing Fe impurities using bulk $Ni(OH)_2$ precipitation. When tested in Fe-free conditions, $Ni(OH)_2$/NiOOH exhibited distinct redox features and showed minimal OER activity until high overpotentials (>400 mV), challenging previous studies that likely included unintentional Fe contamination.[16]

Further structural analysis revealed that the more crystalline β-NiOOH phase was less active for OER than its disordered γ-NiOOH precursor, with the apparent activity of β-NiOOH in earlier reports attributed to Fe incorporation during crystallization. In situ conductivity measurements demonstrated that Fe addition increased film conductivity by over 30 times; however, this alone did not account for the enhanced catalytic performance. Instead, thickness-dependent activity measurements on different substrates supported a partial-charge-transfer interaction between Fe and Ni as the primary activation mechanism. These findings provide critical insights into the electronic and structural contributions of Fe in Ni-based OER catalysts and underscore the importance of controlling Fe content in catalyst design and analysis.[16]

2.6 Research Hypothesis

This literature review provides an overview of the use of nickel catalysts in urea oxidation. As shown, there is more to study in regard to the reaction kinetics and mechanisms within the UOR. Therefore, the following hypothesis is made:

Increasing urea concentration has little to no effect on reaction order and therefore does not improve the reaction kinetics within the UOR on a pure Nickel catalyst. The reaction is diffusion limited at low concentrations of urea and kinetically limited at higher concentrations. UOR depends on the availability of Ni^{3+}, which is supplied by the electrochemical oxidation of Ni^{2+}. This means that UOR is not rate determining at low potentials but can become rate determining at higher potentials where the oxidation of Ni^{2+} proceeds rapidly. Therefore, during the reverse sweep of the UOR, there will be inactive sites on the Nickel catalyst where higher concentrations of urea consume all of the Ni^{3+} species and reduce them back to Ni^{2+}, thereby shutting down the reverse indirect mechanism (Eqn 2.10).

Chapter 3

Methodology

3.1 Overview

This section explains the electrochemical methods used to characterize the urea oxidation reaction on nickel catalysts. The results produced in this paper reflect the controlled processes used to get reproducible results, primarily for collecting cyclic voltammetry (CV) data. These processes come from the electrochemical setup, the preparation of the electrodes, the preparation of the solution, and the programmed electrochemical conditions.

3.2 Electrochemical Cell Setup

All electrochemical experiments were conducted using a standard three-electrode configuration, as illustrated in Figure 3.1. This setup comprised of a nickel “coupon” working electrode, a platinum coil counter electrode, and a Hg/HgO reference electrode. The potential of the working electrode was systematically varied, and the resulting current was measured with respect to the reference electrode. The counter electrode functioned to complete the electrochemical circuit by providing current to the working electrode. All electrodes were controlled using a Solartron 1287A potentiostat, interfaced with a Solartron 1252A frequency response analyzer. This integrated system enabled the performance of a variety of electrochemical techniques, including cyclic voltammetry and potentiostatic hold measurements.

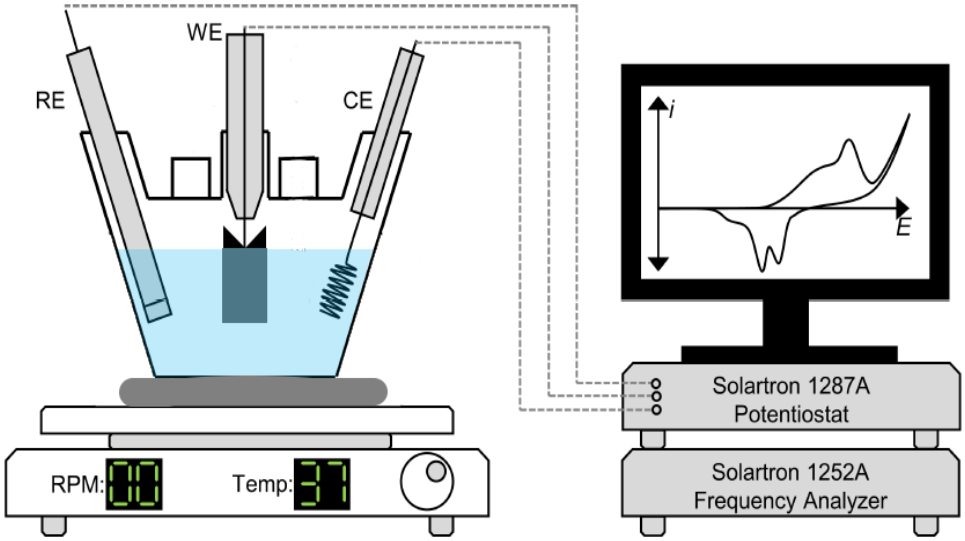

Figure 3.1 Electrochemical Setup. Composed of Electrochemical Cell with Reference Electrode (RE), Working Electrode (WE), and Counter Electrode (CE). Connected to Potentiostat and Frequency Analyzer.

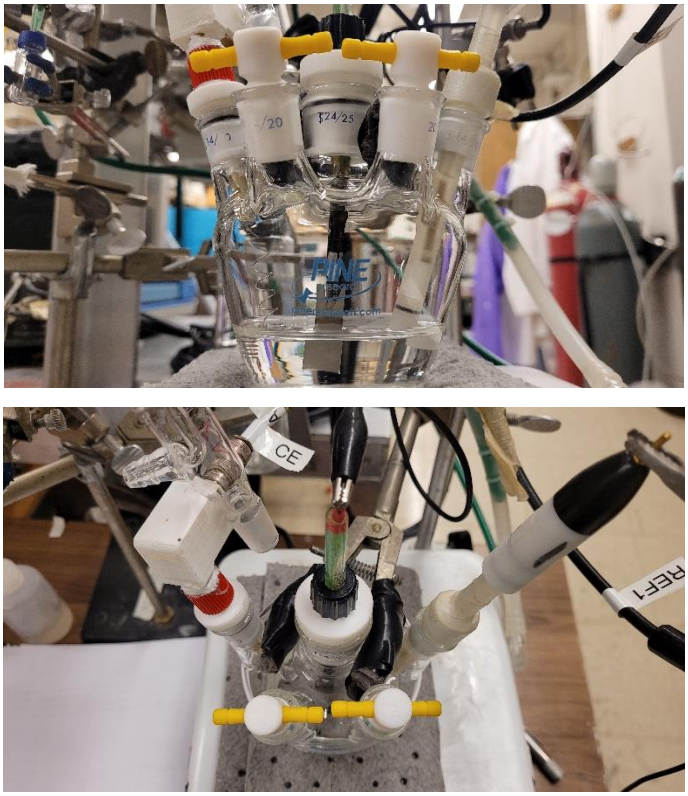

Figure 3.2 Side and Top-Down Views of Electrochemical Setup

3.3 Electrolyte Solution

A supporting electrolyte was employed in the three-electrode cell to facilitate the transport of reactants to the working and counter electrodes and to maintain charge neutrality through ion migration during electrochemical reactions. In this study, potassium hydroxide (KOH) was used as the supporting electrolyte at a concentration of 1 M to ensure high ionic conductivity. A "blank" scan was completed with 1 M KOH in order to set-up a control set to be compared with urea oxidation experiments. For urea oxidation experiments, urea was added to the electrolyte starting at the dialysate-relevant concentrations (10 mM) and then toward higher concentrations (50 mM) in order to evaluate the mass transfer diffusion limitations and its transition toward the reaction kinetics limitations.

Electrolyte solutions were prepared under a fume hood. An initial 50 mL solution of 1 M KOH was prepared by dissolving 2.805 g of solid KOH in 50 mL of deionized (DI) water and was used for baseline cyclic voltammetry (CV) sweeps. For urea oxidation experiments, 25 mL of 1 M KOH was prepared by dissolving 1.403 g of solid KOH in 25 mL of DI water. Urea was then introduced at varying concentrations by first preparing stock solutions; for example, a 10 mM urea solution was obtained by dissolving 15.02 mg of solid urea in 25 mL of DI water. This solution was subsequently mixed with the 1 M KOH to form the final electrolyte for CV experiments. Higher urea concentrations (20 mM and 50 mM) were prepared in the same manner using 30.03 mg and 75.08 mg of solid urea, respectively. Each urea-containing electrolyte was freshly prepared prior to the corresponding CV measurement.

Although previous studies within the research group incorporated protocols to eliminate incidental iron, this procedure was not adopted in the present study. While Trotochaud et al. demonstrated that incidental iron can influence the performance of nickel-based electrocatalysts, it was assumed that variations in urea concentration would produce comparable mass transfer and kinetic limitations regardless of iron presence.[16] As part of a comparative analysis, samples purified according to established protocols were evaluated alongside freshly prepared batches specific to this study. For future investigations seeking greater precision, iron-free preparation methods will be implemented.

3.4 Electrode Preparations

The nickel working electrode (WE) can exhibit a range of electrochemical behaviors depending on their phase composition, surface morphology, and oxide layer thickness. To ensure consistent and reproducible electrochemical responses in alkaline media, the electrode surfaces were standardized by removing surface roughness, eliminating oxide layers, and maintaining a single-phase structure. Metallic electrodes with flat, planar geometries were selected to enable precise control over the electrode surface. These electrodes were polished to a mirror finish to eliminate surface roughness caused by prior experiments or ambient oxide formation. Following polishing, the electrodes were thoroughly rinsed in DI water to remove any residual polishing compounds. A pre-conditioning run was conducted through electrochemical reduction at –0.48 V vs. RHE in alkaline solution to remove any nascent surface oxides according to the study done by Alsabet et al.[14] During electrochemical measurements, a meniscus was formed by carefully raising the electrode and keeping the electrolyte's surface tension, which limited reactions to the defined surface area and enhanced the removal of gaseous products from the electrolyte.

The mercury/mercury oxide reference electrode (RE), filled with 4.24 M KOH and possessing a standard potential of +0.098 V vs. SHE, was prepared and maintained following standard procedures. When not in use, the electrode was stored in its designated storage solution. Prior to use, it was removed from the storage bottle and rinsed thoroughly with DI water. The electrode tip was then polished using a figure-eight motion on the designated polisher to remove any surface impurities or oxide layers. Following polishing, the electrode was rinsed again with DI water. Once cleaned, the electrode was inserted into the electrochemical cell with the tip fully submerged in the electrolyte solution, and the reference electrode wire was connected for use in cyclic voltammetry measurements.

The platinum counter electrode (CE) consisted of a platinum wire coiled at one end and attached to a BNC connector module. Prior to use, the electrode was rinsed thoroughly with DI water to remove any surface contaminants. After rinsing, the electrode was placed into the electrolyte solution and connected to the potentiostat using a BNC coaxial cable. Once properly connected, the electrode was ready for use in cyclic voltammetry experiments.

3.5 Cyclic Voltammetry

Cyclic voltammetry (CV) represents one of the most versatile and informative electroanalytical techniques in modern electrochemistry. This potentiodynamic electrochemical

measurement involves the controlled variation of potential applied to an electrode surface while simultaneously recording the current response. The technique derives its name from the cyclic nature of the potential sweep, wherein the working electrode potential is increased linearly with time until a predetermined switching potential is reached, after which the potential is reversed and decreased to the initial value.[17]

In a typical CV experiment, a potentiostat applies a triangular potential waveform to the working electrode at a constant scan rate (ν). During this process, three critical parameters are continuously measured and recorded: time, applied potential, and the resulting current. The potential is initially increased from a starting value to a predetermined switching potential (E_λ), followed by a reversal to the original potential at the same scan rate. This completes one cycle of the voltametric experiment.

Several characteristic parameters are defined within a cyclic voltammogram to facilitate quantitative analysis and comparison between different electrode systems:

1. **Anodic peak potential ($E_{p,a}$)**: The potential at which maximum oxidation current is observed
2. **Cathodic peak potential ($E_{p,c}$)**: The potential at which maximum reduction current is observed
3. **Half-wave potential ($E_{1/2}$)**: Calculated as the average of anodic and cathodic peak potentials
4. **Onset potential (E_{OS})**: Defined as the potential at which the extrapolated current of a reaction reaches zero

These parameters serve as diagnostic criteria for electrochemical reversibility and provide comparative metrics for evaluating catalytic performance across different electrode materials.

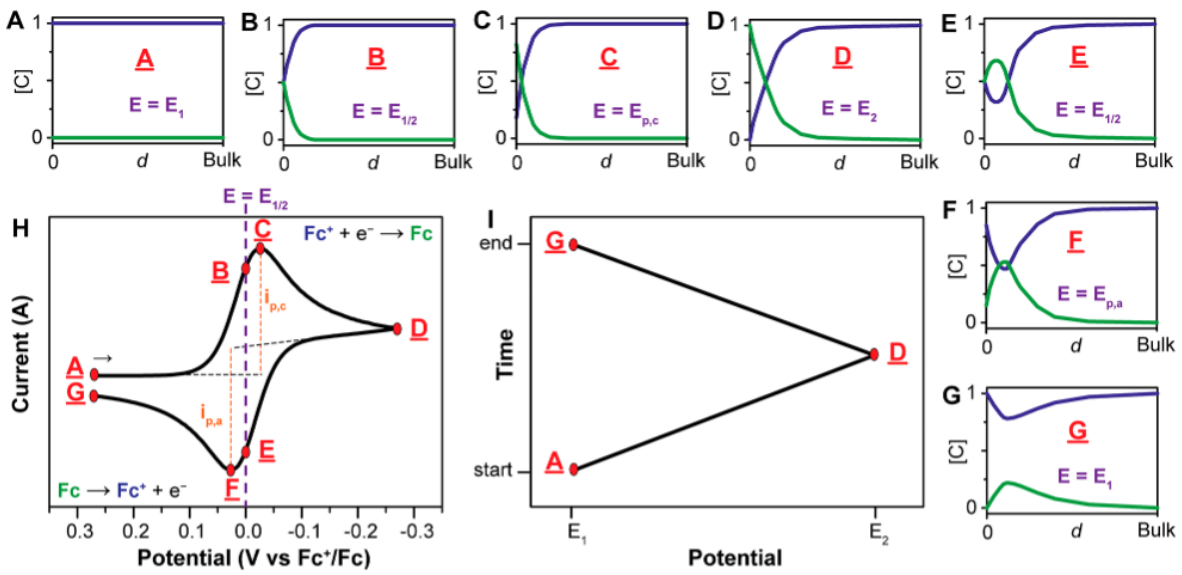

Figure 3.3 Cyclic Voltammetry Breakdown. (A-G) Concentration Profiles with respect to Distance from Electrode. (H) Cyclic Voltammogram. (I) Potential as a Function of Time[18]

CV experiments were conducted using a Solartron potentiostat controlled via the CorrWare software suite. The potentiostat was interfaced with a standard three-electrode electrochemical cell consisting of a nickel working electrode (WE), a coiled platinum wire counter electrode (CE), and a mercury/mercury oxide (Hg/HgO) reference electrode (RE) filled with 4.24 M KOH. The electrolyte solution was an alkaline medium composed of KOH and varying concentrations of urea, prepared immediately prior to each experiment to ensure consistency and avoid degradation.

Before initiating experimental runs, the nickel electrode was electrochemically conditioned through a pre-treatment protocol adapted from the work of Alsabet et al.[14] This preconditioning involved repeated cycling between −1.125 V and −0.0425 V vs. Hg/HgO at a sweep rate of 100 mV s^{-1} under pH 14 conditions.[14] This step was critical to induce the formation of a stable nickel hydroxide/nickel oxyhydroxide surface phase and to ensure the removal of any adsorbed surface contaminants via hydrogen evolution. Cycles were continued until the voltammograms exhibited stable and reproducible profiles, indicating that the surface state of the electrode had reached equilibrium.

Following preconditioning, CV measurements were performed under several experimental schemes to investigate the electrochemical behavior of the nickel electrode in the

presence of urea. These included (i) variable sweep rate experiments, (ii) potential window expansion studies, (iii) electrolyte concentration-dependent studies, and (iv) potential hold studies.

For sweep rate experiments, CV scans were carried out from 0 to 0.65 V vs. Hg/HgO at scan rates of 1, 10, 20, and 100 mV s^{-1}. This allowed for the investigation of electrochemical kinetics and diffusion-limited behavior related to the oxidation of urea and the transformation of nickel hydroxide species.

In the potential window experiments, the upper vertex potential of the voltammetric scan was progressively extended to determine the impact of increasingly oxidative conditions on the electrochemical response of the system. The goal of this set of experiments was to identify the potential thresholds at which side reactions, particularly the oxygen evolution reaction (OER), began to compete with the desired urea oxidation reaction (UOR).

To assess the influence of urea concentration on the CV response, electrolyte solutions were prepared with increasing urea concentrations: 0, 10, 20, 50, 100, 200, and 300 mM. These measurements were conducted in the potential range of 0 to 0.65 V vs. Hg/HgO. A secondary set of concentration experiments was also carried out with urea levels up to 50 mM but using a narrower potential window (0 to 0.55 V vs. Hg/HgO) to further resolve the nickel redox transitions without significant contribution from water oxidation. Due to the necessity of manually preparing fresh electrolyte solutions for each concentration, these trials could not be executed in an automated batch sequence, in contrast to the sweep rate and potential window experiments.

In addition to dynamic cyclic voltammetry measurements, potential hold experiments were performed to further investigate the equilibrium behavior of the nickel electrode during urea electrooxidation. These experiments followed a similar protocol to the urea concentration-dependent CV studies, in which electrolyte solutions containing 0, 10, 20, and 50 mM urea were tested over a potential range of 0 to 0.55 V vs. Hg/HgO. However, instead of completing a continuous potential sweep, the applied potential was held constant at 0.55 V for a duration of one minute at the end of each scan. This modification allowed for observation of steady-state current behavior, offering additional insight into the kinetic and transport-limited aspects of the urea oxidation reaction under quasi-equilibrium conditions. The data obtained from these

potential hold experiments provided critical information on the extent of electrode surface passivation, the stability of the nickel oxyhydroxide phase under prolonged polarization, and the sustained catalytic activity as a function of urea concentration.

Between each experimental set, the electrochemical cell was carefully cleaned and reassembled. Fresh electrolyte solutions were prepared, and the electrodes were rinsed and reconditioned following the same procedures to maintain experimental consistency. Special attention was paid to minimizing excessive hydrogen evolution at high cathodic potentials, which could otherwise alter local pH or damage the integrity of the working electrode surface.

Chapter 4

Results and Discussion

4.1 Introduction

The cyclic voltammograms (CVs) presented in this section serve as the primary electrochemical evidence for the oxidation behavior of nickel-based electrodes in alkaline media, particularly in the presence of urea. Each CV set is depicted across three levels of magnification to facilitate interpretation: (i) a full scan of the potential window to observe the complete electrochemical profile, (ii) a zoomed-in view emphasizing the higher potential region where key oxidation processes occur, and (iii) a detailed visualization of the cathodic sweep, which is of central interest due to its relevance to nickel oxidation kinetics and catalysis.

The cathodic portion of the voltammogram (Figures 4.3 & 4.6) is especially critical as it captures the reduction transitions of nickel oxyhydroxide back to nickel hydroxide species, transitions directly involved in the electrochemical-chemical (EC') mechanism central to urea oxidation. Specifically, this region contains two distinct oxidation peaks attributed to phase transitions: the smaller potential peak corresponds to the γ-NiOOH to α-$Ni(OH)_2$ transformation, while the larger potential peak is associated with the β-NiOOH to β-$Ni(OH)_2$ reduction. This transformation is essential for closing the catalytic cycle in the indirect mechanism of urea oxidation and is governed by equation 2.10. The prominence and position of this peak serve as indicators of the reversibility and electrochemical accessibility of the Ni^{3+}/Ni^{2+} redox couple. In the context of urea electrooxidation, this reaction is particularly significant, as the catalytic role of NiOOH involves its consumption in the chemical oxidation of urea, represented by equation 2.11.

Thus, the cathodic process both reflects the electrochemical regeneration of $Ni(OH)_2$ and serves as an indirect marker of urea oxidation activity. A greater cathodic charge indicates a higher extent of NiOOH formation in the prior anodic sweep, which in turn is modulated by the urea concentration in the electrolyte. Figures 4.3 and 4.6 focuses specifically on this cathodic transition, highlighting the shift and intensity of the reduction peak as a function of urea concentration. These data support the hypothesis that urea reacts chemically with NiOOH during

the forward (anodic) scan, altering the subsequent reduction dynamics during the reverse (cathodic) sweep. As urea concentration increases, a notable modulation in the cathodic peak profile is observed, reflecting both kinetic and equilibrium effects of the coupled electrochemical-chemical (EC') mechanism.

The sections that follow explore these changes in greater detail, analyzing peak positions, current densities, and charge integration to understand how urea influences the Ni redox cycle and the overall electrocatalytic behavior of the system.

4.2 Cyclic Voltammetry Plots

Group 1 Plots (0-0.65 V vs Hg/HgO, 0, 10, 20, 50, 100, 200, and 300 mM Urea)

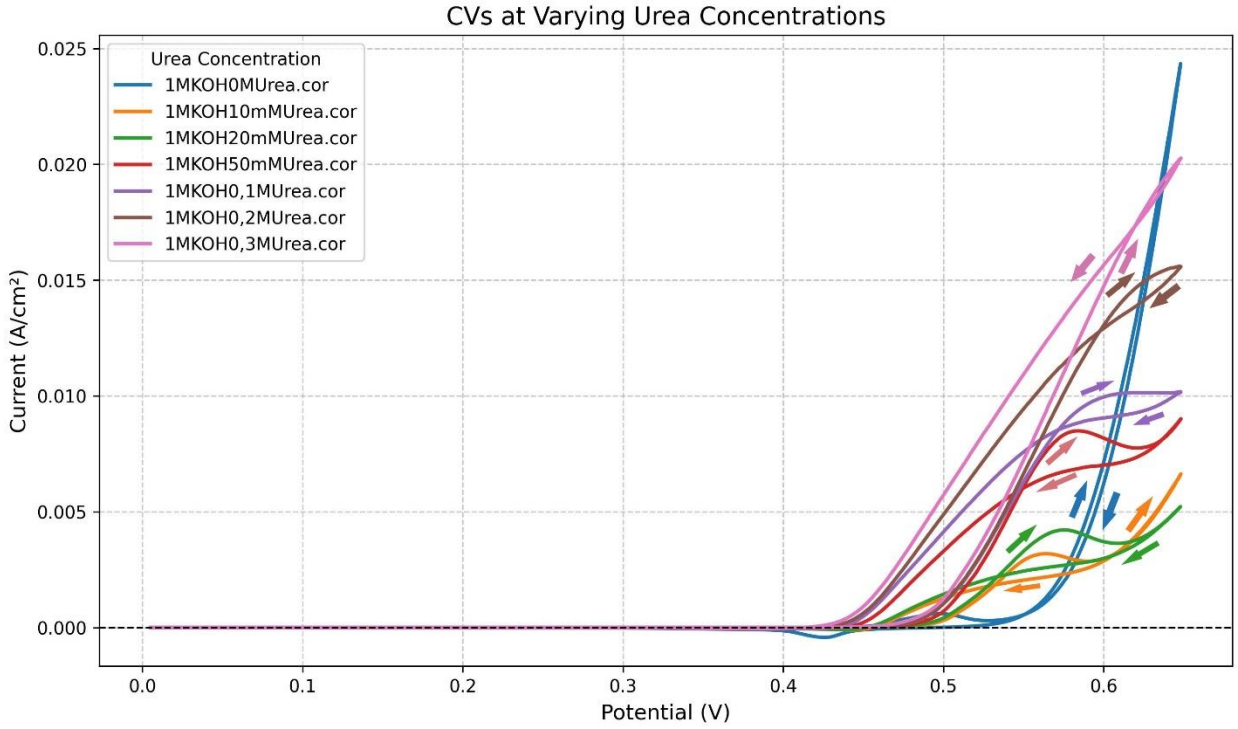

Figure 4.1 Group 1 Full View, Urea concentrations 0 mM (blue), 10 mM (orange), 20 mM (green), 50 mM (red), 100 mM (purple), 200 mM (brown), 300 mM (pink)

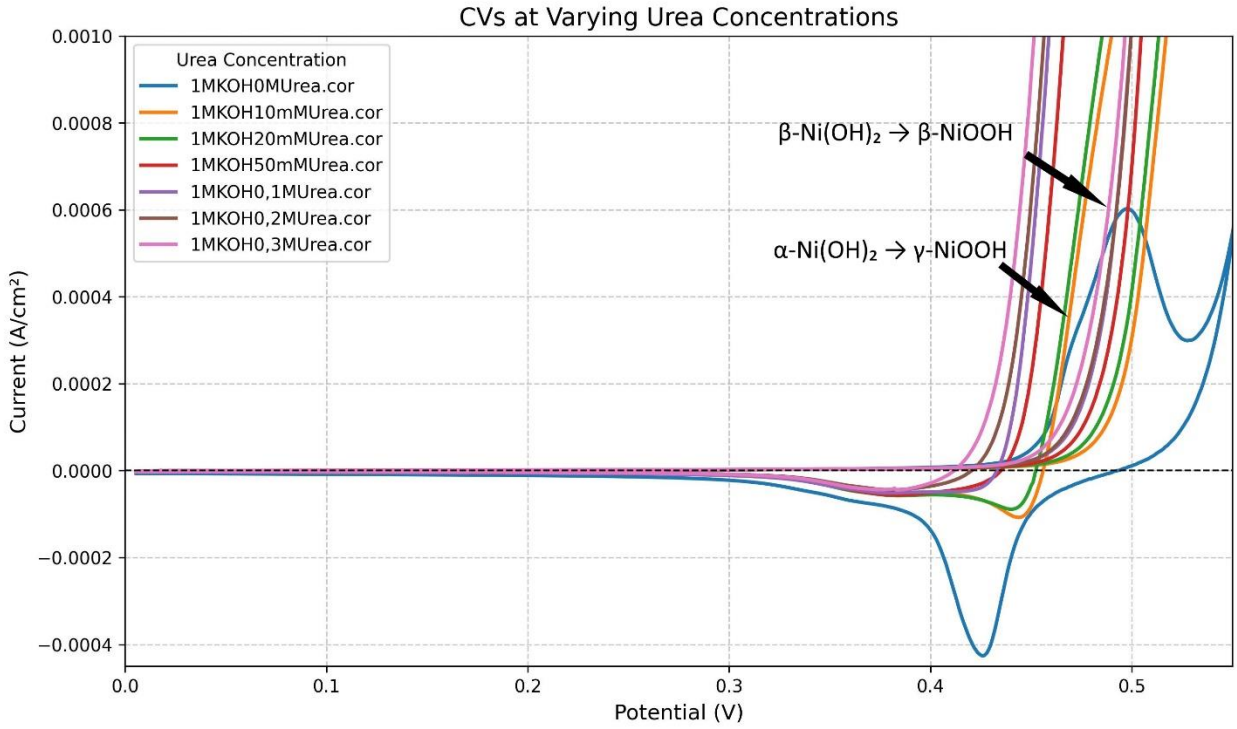

Figure 4.2 Group 1 Partial Zoom, Urea concentrations 0 mM (blue), 10 mM (orange), 20 mM (green), 50 mM (red), 100 mM (purple), 200 mM (brown), 300 mM (pink)

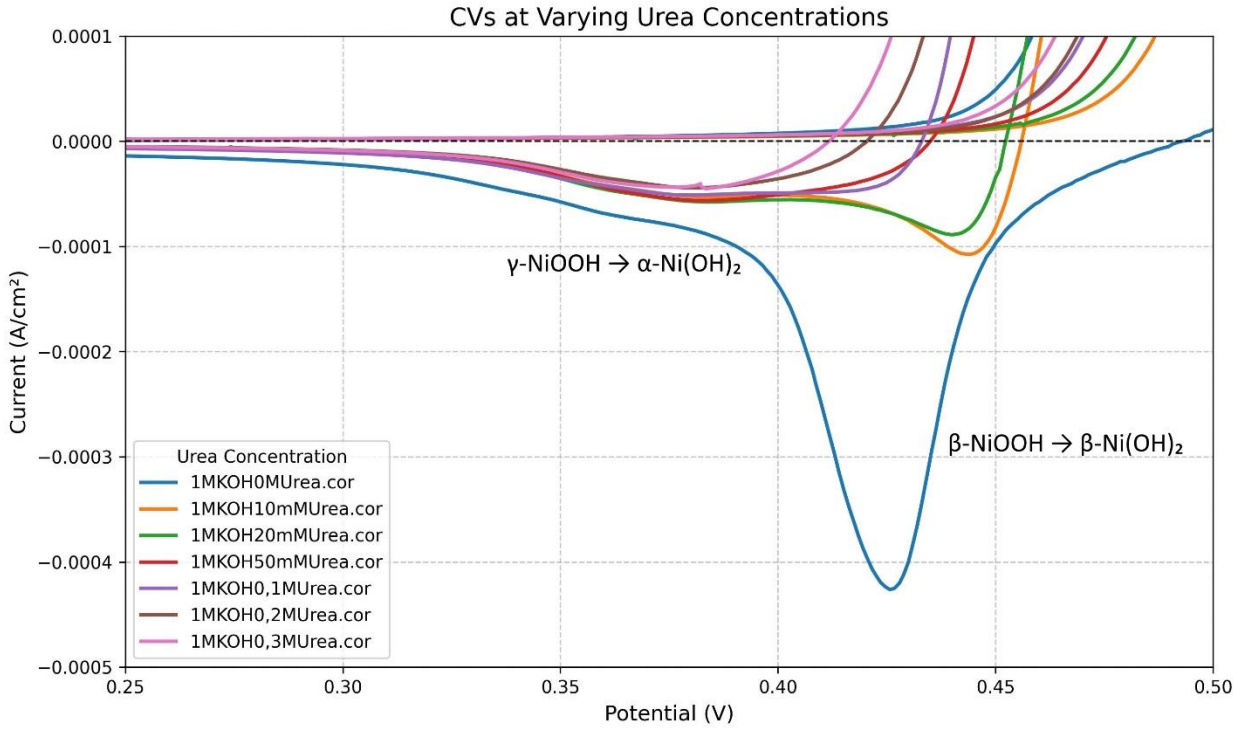

Figure 4.3 Group 1 Cathodic Zoom, Urea concentrations 0 mM (blue), 10 mM (orange), 20 mM (green), 50 mM (red), 100 mM (purple), 200 mM (brown), 300 mM (pink)

Group 2 Plots (0-0.55 V vs Hg/HgO, 0, 10, 20, 50 mM Urea)

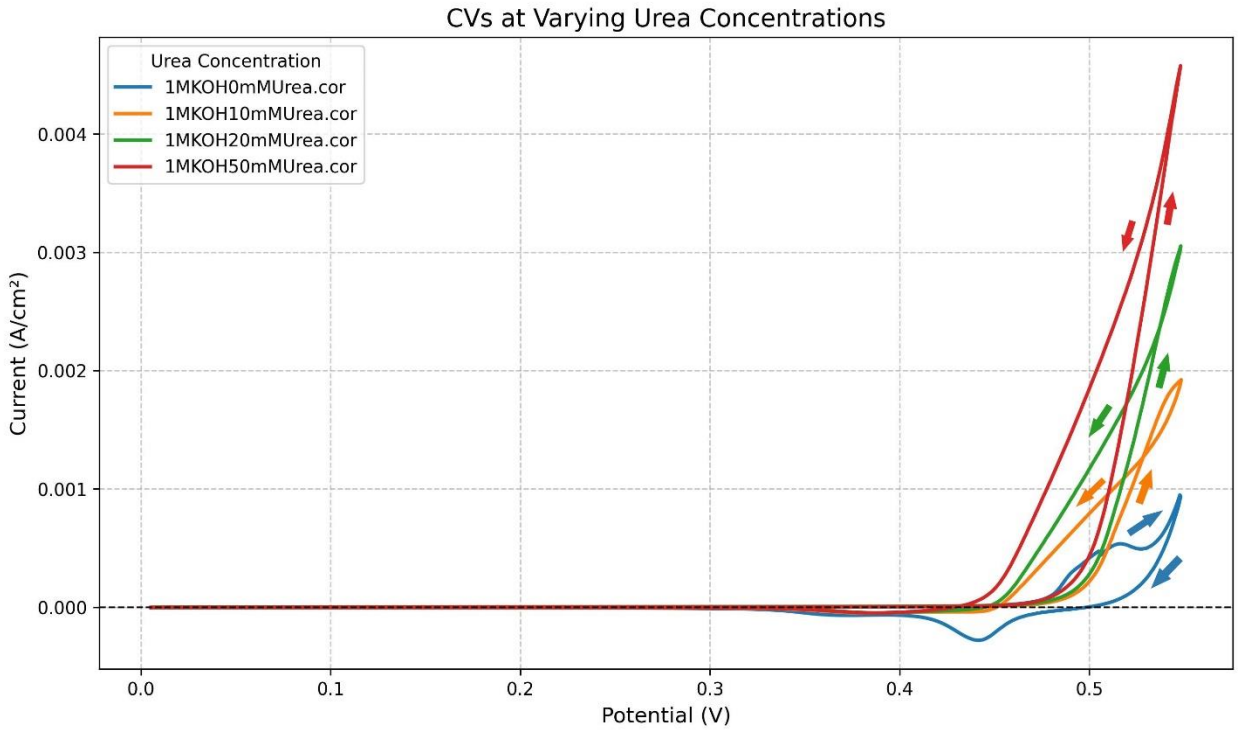

Figure 4.4 Group 2 Full View, Urea concentrations 0 mM (blue), 10 mM (orange), 20 mM (green), 50 mM (red)

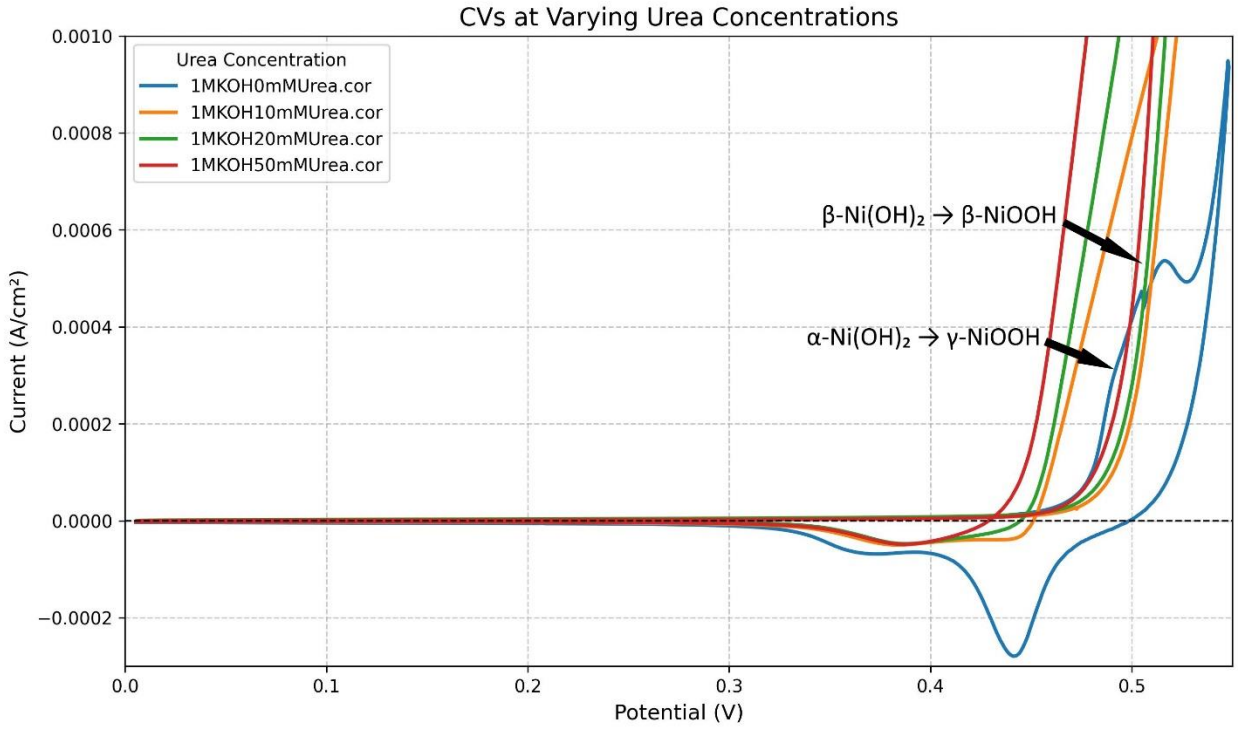

Figure 4.5 Group 2 Partial Zoom, Urea concentrations 0 mM (blue), 10 mM (orange), 20 mM (green), 50 mM (red)

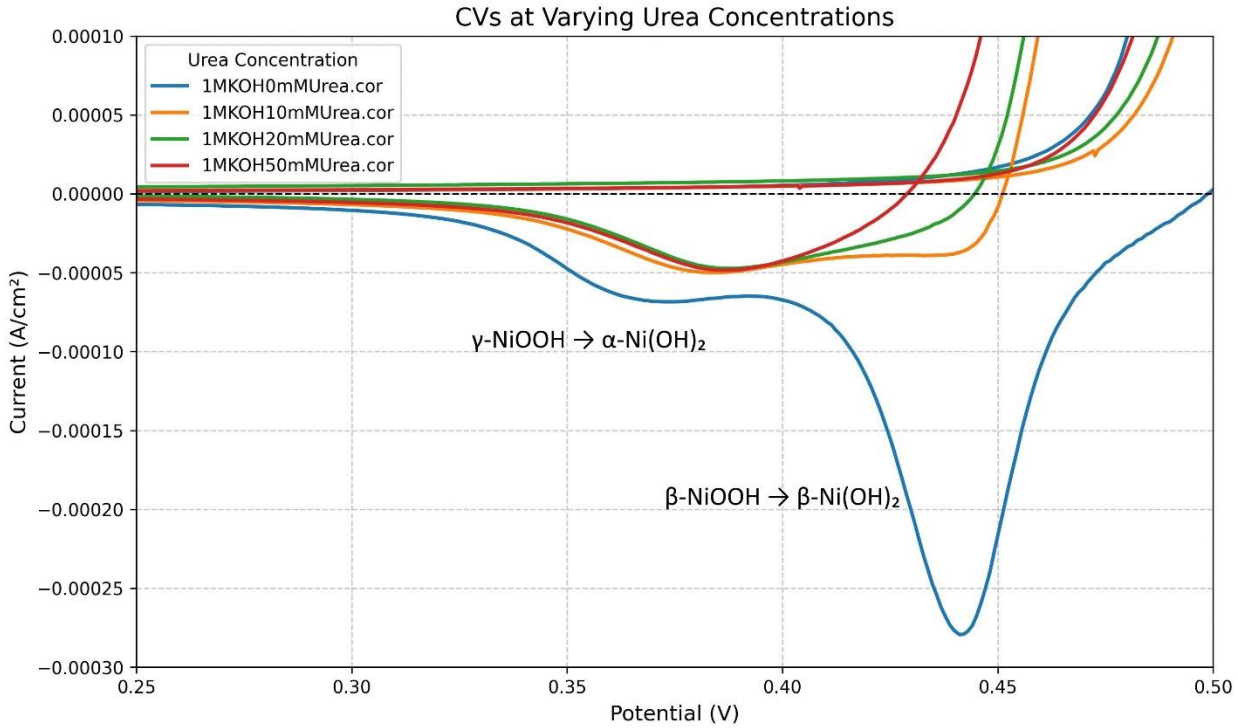

Figure 4.6 Group 2 Cathodic Zoom, Urea concentrations 0 mM (blue), 10 mM (orange), 20 mM (green), 50 mM (red)

4.3 Analysis of Cyclic Voltammetry Plots

Figure 4.1

Figure 4.1 presents the full cyclic voltammetric scans for Group 1, spanning the potential range of 0.00 to 0.65 V vs. Hg/HgO, across varying urea concentrations (0, 10, 20, 50, 100, 200, and 300 mM). Several key electrochemical behaviors are evident from this global perspective. First, the 0 mM urea condition (the blank electrolyte), displays a characteristic rise in current density as the potential approaches 0.65 V, consistent with the onset of the oxygen evolution reaction (OER). In the absence of urea, the anodic scan proceeds uninterrupted toward water oxidation, and the current density at the upper limit is the highest among all scans. This outcome highlights the direct competition between OER and urea oxidation at high anodic potentials.

A second noteworthy observation is the effect of urea on the shape of the voltammograms. The presence of urea induces a pronounced *hysteresis* effect, wherein the cathodic (reverse) scan exhibits higher current densities than the anodic (forward) scan at equivalent potentials. This feature is particularly pronounced at lower urea concentrations (10–50 mM) and becomes less distinct as concentration increases. The hysteresis suggests a kinetic delay or surface activation phenomenon, possibly attributed to the time-dependent chemical interaction between NiOOH and urea. At lower concentrations, the chemical step involving urea oxidation (Equation 2.11) may be slower, allowing accumulation of NiOOH during the forward scan, which is then more rapidly reduced in the reverse scan. At higher urea concentrations, this effect is diminished, likely due to more rapid and continuous consumption of NiOOH throughout the cycle.

Lastly, a clear trend emerges, higher urea concentrations result in elevated anodic currents, particularly beyond ~0.4 V. This observation aligns with enhanced electrocatalytic activity, as more urea is available to react with NiOOH, thus amplifying the overall current response. The increasing slope in current density with urea concentration confirms the electrocatalytic role of NiOOH as an oxidant in the indirect urea oxidation pathway.

Figure 4.2

Figure 4.2 offers a closer examination of the higher potential region of Group 1, emphasizing the anodic peak structure and phase transitions within the nickel hydroxide system. The blank scan (0 mM urea) reveals two prominent oxidation peaks, corresponding to the α-$Ni(OH)_2$ → γ-NiOOH and β-$Ni(OH)_2$ → β-NiOOH transformations. The clarity and symmetry of these redox features in the absence of urea serve as a reference for comparison with modified profiles at increasing urea concentrations.

As urea is introduced, these features become less symmetrical and more distorted, reflecting interference in the reversible redox cycling of the $Ni(OH)_2$/NiOOH couple. This distortion is indicative of a superimposed chemical step, namely the oxidation of urea by NiOOH (Equation 2.11) that consumes the oxidized species before they can be electrochemically reduced during the cathodic sweep. Thus, the shape of the anodic peaks evolves with urea concentration, providing further support for the EC' catalytic mechanism.

Figure 4.3

Figure 4.3 focuses on the cathodic region of Group 1, revealing detailed features associated with the reduction of Ni^{3+} back to Ni^{2+}. Here, the current response of the blank scan is again distinctive, displaying two clear cathodic peaks corresponding to the β-NiOOH → β-$Ni(OH)_2$ and γ-NiOOH → α-$Ni(OH)_2$ transitions. The β-phase reduction peak, generally more negative and higher in magnitude, is especially prominent in the absence of urea.

As urea concentration increases, the β-Ni(III) reduction peak is increasingly suppressed. At high concentrations (≥100 mM), this peak becomes indistinct, suggesting near-complete consumption of β-NiOOH via chemical reaction with urea during the anodic scan. In contrast, the γ-NiOOH → α-$Ni(OH)_2$ transition appears relatively stable across all concentrations, though its current magnitude is reduced in urea-containing scans. These trends provide mechanistic evidence that β-NiOOH is preferentially involved in the catalytic oxidation of urea, while the γ-phase may be less reactive under these conditions.

Figure 4.4

To better isolate the effects of urea at lower overpotentials and avoid complications from OER, Group 2 experiments were conducted within a reduced potential window (0.00–0.55 V vs. Hg/HgO). Figure 4.4 presents full scans for 0, 10, 20, and 50 mM urea. In this narrower window,

the current response of the blank scan is more limited, and the OER current plateau seen in Figure 4.1 is absent. Consequently, the current at 0 mM is no longer the highest, and the catalytic contribution of urea becomes more apparent.

Although the hysteresis effect persists, it is less pronounced, consistent with the reduced availability of NiOOH due to lower anodic potentials. Nevertheless, the trend of increasing current response with increasing urea concentration is still clearly evident, affirming the role of urea as an electroactive species even at reduced driving potentials.

Figure 4.5

Figure 4.5, which zooms into the oxidation region of Group 2, reinforces the trends noted in Group 1. The redox peaks are again distorted in the presence of urea, and the transition from Ni^{2+} to Ni^{3+} phases becomes less distinct. However, these effects are subtler due to the lower maximum applied potential.

Figure 4.6

Figure 4.6 provides a cathodic zoom analogous to Figure 4.3. One notable difference is the relative separation between the 0 and 10 mM urea scans, unlike Group 1, where these scans exhibit similar current magnitudes at the same potential, in Group 2, the 10 mM scan shows a significantly reduced cathodic current. This suggests that even at relatively low urea concentrations, the chemical step can significantly suppress β-NiOOH reduction when the OER is not activated. As in Group 1, the γ-NiOOH → α-$Ni(OH)_2$ transition remains relatively consistent, while the β-Ni^{3+} peak is progressively attenuated with increasing urea, supporting its proposed role in the indirect urea oxidation mechanism.

4.4 Analysis of Current-Concentration Plots

Figure 4.7 presents the current response at discrete fixed potentials (0.40 V to 0.45 V vs. Hg/HgO) as a function of urea concentration for Group 1. Each curve represents a vertical "slice" taken from the CV data at the specified potential, providing insight into the potential-resolved electrochemical behavior of the system.

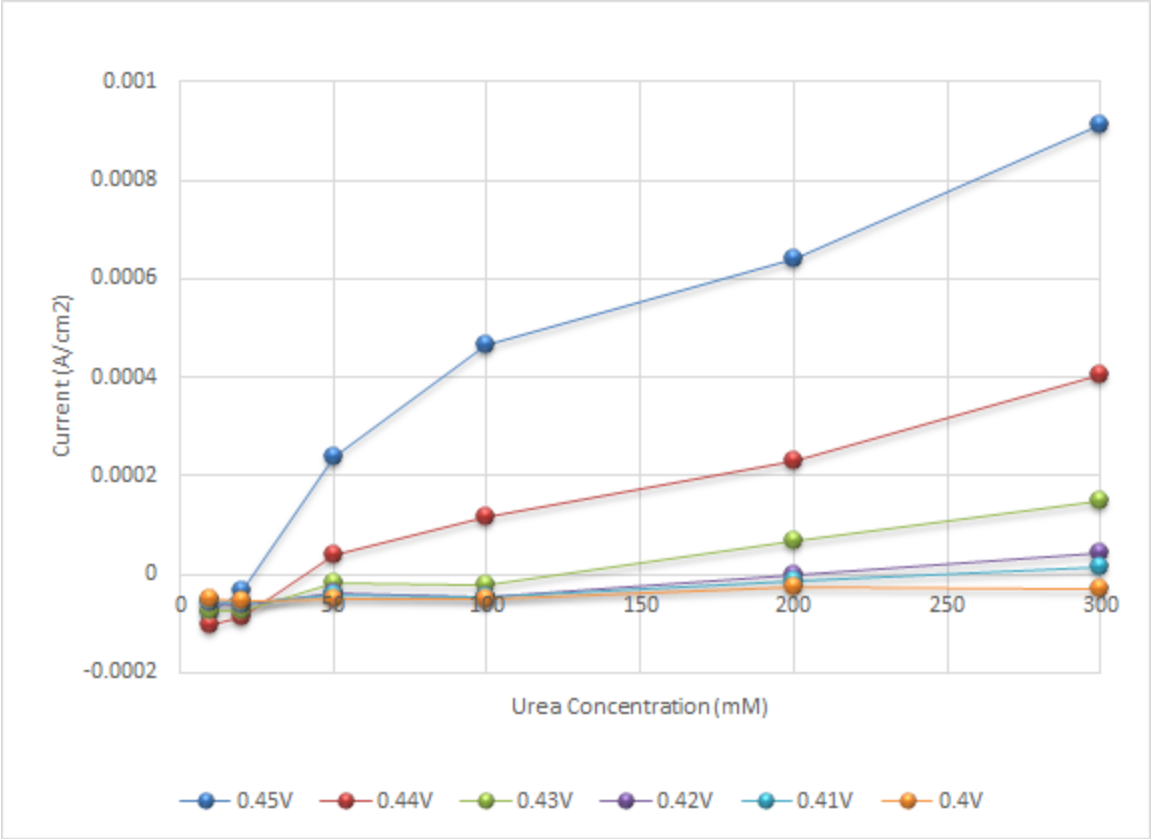

Figure 4.7 Group 1 Cathodic Current Respomse vs Urea Concentration at Fixed Potentials

At lower potentials (0.40–0.42 V), the current remains near zero or slightly negative, suggesting that urea does not significantly participate in the electrochemical process under these conditions. These regions are likely below the threshold required for the oxidative activation of the nickel surface (i.e., formation of NiOOH), and thus minimal catalytic activity is observed.

As the potential increases beyond 0.43 V, the current begins to rise with increasing urea concentration, most notably at 0.44 V and 0.45 V. The rapid, nonlinear increase in current at 0.45 V indicates a highly active electrocatalytic region where NiOOH species are likely present and facilitating the indirect oxidation of urea. This supports the proposed mechanism wherein urea reacts with surface NiOOH species to produce nitrogen, carbon dioxide, and regenerate $Ni(OH)_2$. The curvature and magnitude of the current response suggest that both surface availability and urea concentration contribute to the observed kinetics, with potential contributions from adsorption and transport limitations at higher concentrations.

These fixed-potential concentration plots illustrates the onset behavior and catalytic threshold of the electrode system and reinforce the role of potential in modulating nickel surface phase transitions and the subsequent urea oxidation kinetics.

4.5 Analysis of Cathodic Area

Figures 4.8 and 4.9 present the cathodic area extracted from the cyclic voltammograms for Group 1 and Group 2, respectively. The cathodic area corresponds to the integrated region of negative current observed during the reverse scan, which primarily encompasses reductive processes, including the transformation of higher-valent nickel species back to lower oxidation states. In the absence of urea, both groups exhibit the largest cathodic areas, indicative of pronounced reduction currents likely associated with the β-NiOOH to β-$Ni(OH)_2$ transition.

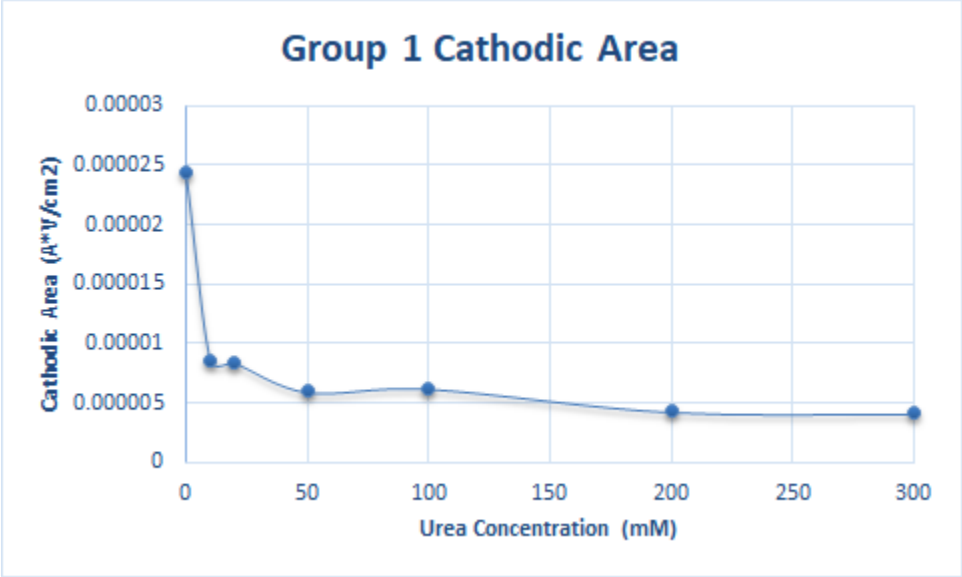

Figure 4.8 Integrated Cathodic Area of Group 1

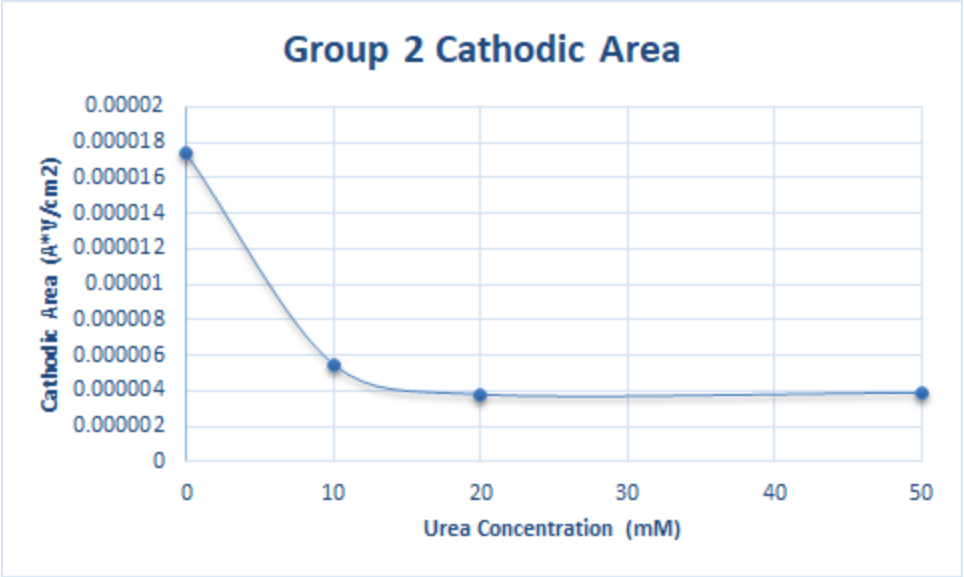

Figure 4.9 Integrated Cathodic Area of Group 2

Upon introduction of urea, a sharp and immediate decline in cathodic area is observed in both groups. This trend signifies that urea strongly suppresses the reverse scan reduction process, which is consistent with previous interpretations that urea interferes with or delays the NiOOH reduction pathway. The suppression of the β–β peak can be attributed to urea's consumption of Ni^{3+} species during the forward scan, thereby limiting the availability of reducible NiOOH species in the reverse sweep. As urea concentration increases beyond 10–20 mM, the cathodic area plateaus, suggesting that the initial effect saturates and that any remaining cathodic features, such as those related to the γ–α $Ni(OH)_2$/NiOOH transitions, are not significantly affected by further increases in urea concentration. These residual peaks, being less intense and less sensitive to urea, maintain a consistent baseline response across the higher concentration range.

This tapering behavior reinforces the notion that urea's primary influence lies in quenching the dominant β–β peak, while other redox features remain comparatively stable. It also supports the hypothesis that at elevated urea concentrations, the nickel surface remains predominantly in the reduced state during the reverse scan due to the depletion of oxidized nickel species, thus preventing full restoration of the original voltammetric profile.

4.6 Analysis of Ratio of UOR Current Densities

To investigate the potential-dependent kinetics of urea electrooxidation on the nickel electrode, the ratio of background-corrected current responses at 100 mM and 50 mM urea concentrations was plotted as a function of applied potential (Figure 4.10). This approach allows for the assessment of concentration dependence in different potential regimes, providing insight into the nature of the rate-determining step (RDS) across the electrochemical window.

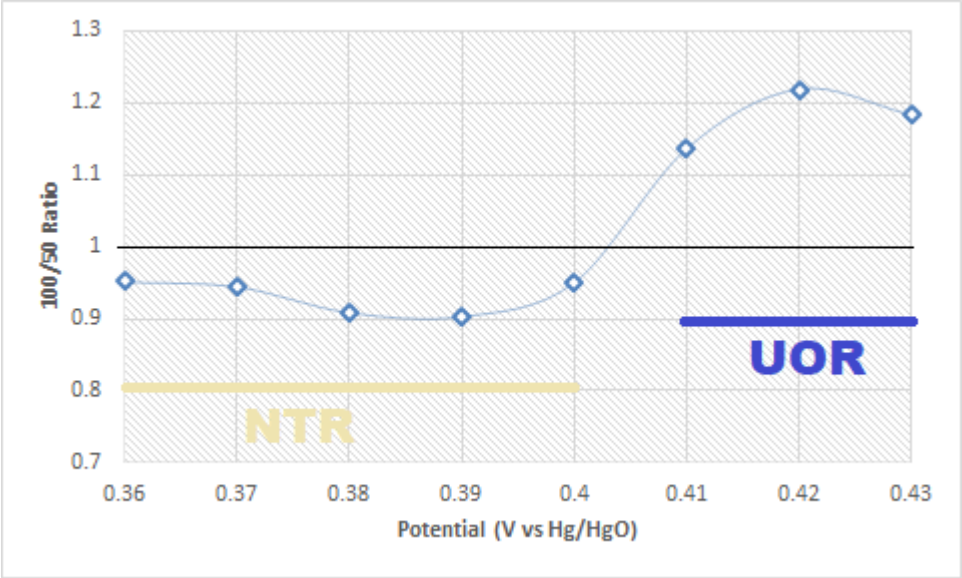

Figure 4.10 Group 1 Ratio of UOR Current Densities at 100 mM and 50 mM Urea Concentrations as a Function of Potential (NTR- Nickel Transition, UOR- Urea Oxidation Reaction)

At lower potentials, ranging approximately from 0.36 V to 0.39 V vs Hg/HgO, the ratio hovers around 0.9–1.0, suggesting negligible dependence of the oxidation current on urea concentration. In this regime, the current is dominated by processes unrelated to urea oxidation or by a step that is not kinetically limited by urea availability. This behavior indicates that the rate-determining step does not directly involve urea as a reactant, which aligns with the mechanistic hypothesis that the $Ni^{2+} \leftrightarrow Ni^{3+}$ redox transition is the limiting process at these lower overpotentials. As this transition is a surface-confined process, the urea concentration in solution has little influence on the observed current, resulting in a near-unity ratio.

A marked change is observed beginning around 0.40 V, where the ratio begins to increase, reaching a maximum of approximately 1.22 at 0.42 V. This upward trend signals a shift in the RDS to one that is increasingly dependent on urea concentration. In this potential region,

the Ni^{3+} species formed at the electrode surface likely becomes available to chemically oxidize urea, making the overall rate of the UOR sensitive to the concentration of urea in solution. The deviation of the ratio from 1.0 towards 2.0, expected for a true first-order reaction, suggests that the chemical step involving urea adsorption or reaction with surface NiOOH is becoming kinetically significant, but may still be influenced by additional complexities such as intermediate surface coverage effects or mass transport limitations.

This transition confirms a mechanistic crossover from a region dominated by the electrochemical Ni^{2+}/Ni^{3+} redox equilibrium to one where the subsequent chemical reaction with urea increasingly dictates the reaction rate. Notably, this analysis supports the interpretation that coupling UOR kinetics with the redox behavior of the Ni electrode enables quantification of the forward rate constant k_f for the $Ni^{2+} \rightarrow Ni^{3+}$ transition under catalytic turnover conditions. Once k_f is established via the urea-mediated enhancement of current, the reverse rate constant k_r can be inferred through comparison with the reversible scan behavior in the absence of urea, allowing a full kinetic characterization of the redox cycle under operando conditions.

4.5 Kinetic Modelling

To quantitatively interpret the potential-dependent behavior of the urea oxidation reaction (UOR) on nickel electrodes, a kinetic model based on surface coverages of active redox states was applied. In this model, k_1 and k_2 are the forward and reverse reactions of (equation 2.10) respectively while k_3 is (equation 2.11). Additionally, θ_2 and θ_3 are the fractional coverages of the $Ni(OH)_2$ and NiOOH respectively. C_W is the activity of water while C_U is the urea concentration. Finally, n and m are the reaction orders of urea and NiOOH respectively.

According to previous literature-derived mechanism, the UOR proceeds via a chemically coupled electron-transfer pathway involving the $Ni(OH)_2$/NiOOH redox pair.[19] The surface coverage of NiOOH (θ_3), which acts as the catalytic oxidant for urea, is governed by the following rate balance equation:

$$\frac{d\theta_2}{dt} = -k_1\theta_2[OH^-] + k_2\theta_3 C_w + 6k_3 C_U^n \theta_3^m = 0 \qquad (4.3)$$

with the site balance constraint $\theta_2 + \theta_3 = 1$. Solving for θ_3 yields:

$$\theta_3 = \frac{k_1[OH^-]}{k_1[OH^-] + k_2 C_w + 6k_3 C_U^n} \qquad (4.4)$$

Assuming m=1, the rate of the chemical UOR step becomes:

$$r_3 = k_3 C_U^m \theta_3 = \frac{k_1 k_3 [OH^-] C_U^n}{k_1 [OH^-] + k_2 C_w + 6 k_3 C_U^n} \quad (4.5)$$

This expression allows two limiting cases to be considered:

1. **Low Potential (Small k_1 Limit):**
   At low applied potentials, the rate constant k_1 for the $Ni(OH)_2 \rightarrow NiOOH$ electrochemical step is small, limiting the overall reaction rate. In this case, the UOR rate simplifies to:

$$r_3 \approx \frac{1}{6} k_1 [OH^-] \quad (4.6)$$

   Here, r_3 becomes independent of urea concentration, and thus the current ratio between 100 mM and 50 mM urea conditions is expected to be unity:

$$\frac{r_3(100\ mM)}{r_3\ (50\ mM)} \approx 1 \quad (4.7)$$

This prediction is consistent with the experimentally observed plateau in the ratio plot (Figure 4.12) at potentials below ~0.40 V vs Hg/HgO, where the ratio remains close to 1.

2. **High Potential (Large k_1 Limit):**
   At higher potentials, k_1 becomes large and no longer limits the UOR rate. The reaction rate then transitions to:

$$r_3 \approx k_3 C_U^n \quad (4.8)$$

   which reflects first-order dependence on urea concentration (if n=1). In this regime, the theoretical ratio of reaction rates for two concentrations is:

$$\frac{r_3(100\ mM)}{r_3\ (50\ mM)} \approx \left(\frac{100}{50}\right)^n = 2^n$$

The experimental data shows an increasing trend in this ratio, reaching values above 1.2 by ~0.42 V, indicating a growing dependence on urea concentration. Although the measured ratio does not fully reach the ideal value of 2, this deviation may result from either a sub-unity

reaction order n<1, partial surface saturation, or concurrent limitations due to intermediate species coverage (i.e., nonlinear θ_3 response).

Together, this analysis provides strong evidence of a kinetic transition in the UOR mechanism: from a potential-controlled Ni^{2+}/Ni^{3+} redox step at low overpotentials to a urea-concentration-dependent chemical step at higher potentials. This crossover illustrates how kinetic modeling, anchored in fractional surface coverage theory, can be used to quantitatively interpret electrochemical rate behavior, particularly when paired with diagnostic metrics such as the current ratio at varying concentrations.

Chapter 5

Conclusion

This study investigated the electrochemical behavior of nickel electrodes in alkaline media for the purpose of elucidating the mechanistic and kinetic characteristics of the urea oxidation reaction (UOR). Through a systematic combination of cyclic voltammetry (CV) and controlled variation of experimental parameters, including urea concentration, potential window, and potential hold conditions, valuable insights were obtained regarding the interaction between urea and the $Ni(OH)_2$/NiOOH redox couple.

The CV data revealed distinct changes in both anodic and cathodic current responses with increasing urea concentration. Notably, suppression of the cathodic β-NiOOH to β-$Ni(OH)_2$ reduction peak at higher concentrations provided strong evidence for the indirect mechanism of urea oxidation, wherein NiOOH acts as a transient oxidant that is chemically reduced by urea before it can be electrochemically regenerated. The effect of urea in this suppression could be greatly seen with the integrated plots of cathodic current. This inhibitory behavior was especially pronounced in the narrower potential window (0–0.55 V vs Hg/HgO), suggesting potential-dependent modulation of catalytic activity.

Moreover, fixed-potential current-concentration profiles and current density ratio analyses demonstrated a clear kinetic crossover. At lower potentials, the system was predominantly governed by the $Ni(OH)_2$ to NiOOH redox transition, with little dependence on urea concentration. At higher potentials (≥0.42 V vs Hg/HgO), the kinetics shifted toward urea-concentration-dependent behavior, consistent with the onset of the chemical oxidation step mediated by surface NiOOH. This trend was well captured by the kinetic model derived from fractional surface coverage theory, validating the mechanistic framework and supporting the hypothesis that UOR activity transitions from redox-limited to chemically limited as a function of applied potential.

While the current work provides mechanistic clarity on the role of NiOOH in urea oxidation and its modulation by concentration and potential, it also opens up several promising avenues for future investigation. First, extending the potential window beyond 0.65 V vs

Hg/HgO would allow for direct exploration of the oxygen evolution reaction (OER) onset and its competition with UOR, particularly under high urea concentrations where surface saturation effects are likely. Second, collecting a broader set of cyclic voltammograms under varying temperatures, scan rates, and electrode morphologies would strengthen the generalizability of the observed trends. Third, incorporation of complementary electrochemical techniques, such as electrochemical impedance spectroscopy (EIS), could provide time-resolved information on charge-transfer resistances and double-layer capacitances, thereby distinguishing between adsorption-limited and electron-transfer-limited processes.

Additionally, coupling the electrochemical measurements with online gas detection techniques, such as differential electrochemical mass spectrometry (DEMS) or gas chromatography, would enable direct quantification of evolved gases (e.g., H_2, N_2, CO_2) and offer real-time validation of proposed reaction pathways. Finally, applying this kinetic framework to alternative Ni-based materials, including doped catalysts and layered double hydroxides, could uncover material-specific effects that enhance UOR activity or selectivity.

In conclusion, this work advances the fundamental understanding of urea electrooxidation on nickel electrodes by bridging electrochemical observables with mechanistic theory. It underscores the nuanced relationship between surface redox dynamics and urea interaction, while laying the groundwork for future studies aimed at optimizing nickel-based catalysts for sustainable hydrogen production and wastewater remediation.

Bibliography

(1) *2024 was the world's warmest year on record | National Oceanic and Atmospheric Administration*. https://www.noaa.gov/news/2024-was-worlds-warmest-year-on-record (accessed 2025-04-30).

(2) *Heraeus_Hydrogen_01_Ubersicht_Horizontal.jpg (1648×824)*. https://www.heraeus-group.com/.imaging/mte/default/1648/dam/group/media_group/news-and-stories/innovation-2022/hydrogen/Heraeus_Hydrogen_01_Ubersicht_Horizontal.jpg/jcr:content/Heraeus_Hydrogen_01_Ubersicht_Horizontal.jpg (accessed 2025-05-12).

(3) Li, J.; Zhang, J.; Yang, J.-H. Research Progress and Applications of Nickel-Based Catalysts for Electrooxidation of Urea. *Int. J. Hydrog. Energy* **2022**, *47* (12), 7693–7712. https://doi.org/10.1016/j.ijhydene.2021.12.099.

(4) Vedharathinam, V.; Botte, G. G. Direct Evidence of the Mechanism for the Electro-Oxidation of Urea on Ni(OH)2 Catalyst in Alkaline Medium. *Electrochimica Acta* **2013**, *108*, 660–665. https://doi.org/10.1016/j.electacta.2013.06.137.

(5) *Eutrophication-Process-1-550x413.png (550×413)*. https://earthhow.com/wp-content/uploads/2017/07/Eutrophication-Process-1-550x413.png (accessed 2025-05-12).

(6) Boggs, B. K.; King, R. L.; Botte, G. G. Urea Electrolysis: Direct Hydrogen Production from Urine. *Chem. Commun.* **2009**, No. 32, 4859. https://doi.org/10.1039/b905974a.

(7) Vedharathinam, V.; Botte, G. G. Understanding the Electro-Catalytic Oxidation Mechanism of Urea on Nickel Electrodes in Alkaline Medium. *Electrochimica Acta* **2012**, *81*, 292–300. https://doi.org/10.1016/j.electacta.2012.07.007.

(8) *urea-molecule-molekuul.jpg (900×800)*. https://images.fineartamerica.com/images-medium-large-5/urea-molecule-molekuul.jpg (accessed 2025-05-12).

(9) Oshchepkov, A. G.; Braesch, G.; Bonnefont, A.; Savinova, E. R.; Chatenet, M. Recent Advances in the Understanding of Nickel-Based Catalysts for the Oxidation of Hydrogen-Containing Fuels in Alkaline Media. *ACS Catal.* **2020**, *10* (13), 7043–7068. https://doi.org/10.1021/acscatal.0c00101.

(10) Abdel Rahim, M. A.; Abdel Hameed, R. M.; Khalil, M. W. Nickel as a Catalyst for the Electro-Oxidation of Methanol in Alkaline Medium. *J. Power Sources* **2004**, *134* (2), 160–169. https://doi.org/10.1016/j.jpowsour.2004.02.034.

(11) Liu, C.; Yang, F.; Schechter, A.; Feng, L. Recent Progress of Ni-Based Catalysts for Methanol Electrooxidation Reaction in Alkaline Media. *Adv. Sens. Energy Mater.* **2023**, *2* (2), 100055. https://doi.org/10.1016/j.asems.2023.100055.

(12) A STUDY OF ALDEHYDE OXIDATION AT GLASSY CARBON, MERCURY, COPPER, SILVER, GOLD AND NICKEL ANODES.

https://pdf.sciencedirectassets.com/280368/1-s2.0-S0022072879X83556/1-s2.0-S0022072879803629/main.pdf.

(13) Huang, J.-J.; Hwang, W.-S.; Weng, Y.-C.; Chou, T.-C. Transformation Characterization of Ni(OH)₂/NiOOH in Ni-Pt Films Using an Electrochemical Quartz Crystal Microbalance for Ethanol Sensors. *Mater. Trans.* **2010**, *51* (12), 2294–2303. https://doi.org/10.2320/matertrans.M2010079.

(14) *Electrochemical Growth of Surface Oxides on Nickel. Part 3: Formation of β-NiOOH in Relation to the Polarization Potential, Polarization Time, and Temperature | Electrocatalysis*. https://link.springer.com/article/10.1007/s12678-014-0214-1 (accessed 2025-04-30).

(15) Plevová, M.; Hnát, J.; Bouzek, K. Electrocatalysts for the Oxygen Evolution Reaction in Alkaline and Neutral Media. A Comparative Review. *J. Power Sources* **2021**, *507*, 230072. https://doi.org/10.1016/j.jpowsour.2021.230072.

(16) Trotochaud, L.; Young, S. L.; Ranney, J. K.; Boettcher, S. W. Nickel–Iron Oxyhydroxide Oxygen-Evolution Electrocatalysts: The Role of Intentional and Incidental Iron Incorporation. *J. Am. Chem. Soc.* **2014**, *136* (18), 6744–6753. https://doi.org/10.1021/ja502379c.

(17) Bard, A.; Faulkner, L. *Electrochemical Methods: Fundamentals and Applications, 2nd Edition | Wiley*, 2nd ed.; Wiley.

(18) Elgrishi, N.; Rountree, K. J.; McCarthy, B. D.; Rountree, E. S.; Eisenhart, T. T.; Dempsey, J. L. A Practical Beginner's Guide to Cyclic Voltammetry. *J. Chem. Educ.* **2018**, *95* (2), 197–206. https://doi.org/10.1021/acs.jchemed.7b00361.

(19) Hopsort, G.; Latapie, L.; Groenen Serrano, K.; Loubière, K.; Tzedakis, T. Indirect Urea Electrooxidation by Nickel(III) in Alkaline Medium: From Kinetic and Mechanism to Reactor Modeling. *AIChE J.* **2023**, *69* (9), e18113. https://doi.org/10.1002/aic.18113.